

EXHAUST GAS ENERGY RECLAMATION WITH A PNEUMATIC BOOST CONVERTER

By

Tyler Gibson

Thesis

Submitted to the Faculty of the
Graduate School of Vanderbilt University

in partial fulfillment of the requirements

for the degree of

MASTER OF SCIENCE

in

MECHANICAL ENGINEERING

August 11, 2017

Nashville, Tennessee

Approved:

Eric J. Barth, Ph.D.

Kenneth Frampton, Ph.D.

Michael Goldfarb, Ph.D.

ACKNOWLEDGMENTS

I would like to express my sincerest thanks to my advisor, Dr. Eric Barth, for the opportunity to work on this project with him. His guidance was integral to the research conducted and presented by this thesis. Additional thanks to my colleagues in the Laboratory for the Design and Control of Energetic Systems, with special thanks to Seth Thomas, for his assistance with setting up my data acquisition system, and Bryn Pitt, for his aid and guidance in the machine shop. I would also like to express my gratitude to the members of my thesis committee: Dr. Frampton and Dr. Goldfarb.

Furthermore, I would like to thank my family and friends for their support and encouragement through my research. Their advice and direction was very helpful and always appreciated.

Finally, special thanks to the National Fluid Power Association for the funding necessary to support this research.

TABLE OF CONTENTS

| | Page |
|---|------|
| ACKNOWLEDGMENTS..... | ii |
| LIST OF FIGURES | v |
| LIST OF TABLES | vii |
| Chapter | |
| I. Overview | 1 |
| Introduction and Motivation | 1 |
| Literature Survey | 2 |
| Organization of the Document..... | 5 |
| References | 5 |
| II. Manuscript 1: Dynamic Equivalence of Pneumatic and Electrical Boost Converters for Exhaust Gas Energy Reclamation | 7 |
| Abstract..... | 8 |
| Nomenclature | 8 |
| Introduction | 9 |
| Electrical Boost Converter | 10 |
| Pneumatic Boost Converter..... | 14 |
| Modeling Results | 16 |
| Conclusions and Future Work | 21 |
| Acknowledgments..... | 22 |
| References | 22 |
| III. Manuscript 2: Design, Model, and Experimental Validation of a Pneumatic Boost Converter | 23 |
| Abstract..... | 24 |
| Introduction | 24 |
| Design..... | 25 |
| Dynamic Model | 29 |
| A. Pressure Dynamics | 29 |
| B. Mass Flow..... | 30 |
| C. Device Description..... | 31 |
| D. Energy | 32 |
| Experimental Validation of the Model..... | 34 |

| | |
|--|----|
| A. Experimental Setup | 34 |
| B. Boost Converter Parameters | 36 |
| C. Effective Damping | 37 |
| D. Experimental vs. Simulated Pressures..... | 37 |
| E. Energy Reclamation and Efficiency..... | 33 |
| Conclusion | 44 |
| Acknowledgment | 45 |
| References | 45 |
| IV. Future Directions | 47 |
| Appendix | |
| A: Simulink Diagrams..... | 48 |
| B: Matlab Code | 55 |
| Dynamic Model Parameters | 55 |
| PSI to kPa Function..... | 57 |
| PSI to kPa Function..... | 57 |
| Figure Creation Script..... | 57 |
| Plot Simulated and Experimental Results | 57 |
| Overlay Consecutive Experimental Results | 58 |
| Extract Data from Target Machine, Plot, and Save | 60 |
| C: Prototype Technical Drawings..... | 61 |
| D: Data Acquisition..... | 65 |

LIST OF FIGURES

| Figure | Page |
|---|------|
| 1 - 1: Pneumatic actuation and exhaust to atmosphere..... | 2 |
| 1 - 2: Strain energy accumulator demonstration platform | 3 |
| 1 - 3: Pneumatic boost converter schematic | 4 |
| 2 - 1: Circuit diagram of an electrical boost converter..... | 10 |
| 2 - 2: Voltage across the load when the boost converter switch is opened. The supply voltage is 12V | 11 |
| 2 - 3: Current in inductor charging while the switch is closed and discharging when the switch is opened at $t=0.05s$ | 12 |
| 2 - 4: Energy exchange between the inductor and capacitor showing the charging of the inductor and discharge across the load | 13 |
| 2 - 5: Zoom plot of energy exchange occurring when the switch is opened | 13 |
| 2 - 6: Diagram of proposed Pneumatic Boost Converter | 15 |
| 2 - 7: The pressure spike experienced in V_2 when the ball passes the vent, sealing it | 17 |
| 2 - 8: The velocity of the ball \dot{z} through one energy exchange cycle | 18 |
| 2 - 9: Maximum energy reclaimed by various combinations of tube lengths | 19 |
| 2 - 10: Pneumatic energy exchange between the two potential pressure energies, the kinetic energy of the ball, and the energy being reclaimed through the check valve..... | 20 |
| 2 - 11: Zoomed view of the first three cycles of the pneumatic energy exchange | 20 |
| 3 - 1: Circuit diagram of an electrical boost converter..... | 26 |
| 3 - 2: Pneumatic boost converter prototype schematic..... | 27 |
| 3 - 3: Pneumatic boost converter bond graph | 28 |
| 3 - 4: Annotated photograph of the pneumatic boost converter with close-up views of the adjuster, vent, and system inlet | 35 |
| 3 - 5: Experimental and simulated exhaust pressures with roughly..... | 39 |
| 3 - 6: Experimental and simulated tank pressures with roughly..... | 39 |
| 3 - 7: Experimental and simulated exhaust pressures with roughly..... | 40 |
| 3 - 8: Experimental and simulated tank pressures with roughly..... | 40 |
| 3 - 9: Experimental and simulated exhaust pressures with roughly..... | 41 |
| 3 - 10: Experimental and simulated tank pressures with roughly..... | 41 |
| 3 - 11: Experimental exhaust pressures from six consecutive actuations overlaid..... | 42 |
| 3 - 12: Experimental tank pressures from six consecutive actuations overlaid | 42 |

| | |
|--|----|
| 3 - 13: Experimental and simulated results at 653 kPa (80 psig) supply | 43 |
| A - 1: Simulink model overview..... | 48 |
| A - 2: Volume calculations and energy of ball | 49 |
| A - 3: Force balance on ball and acceleration integration | 49 |
| A - 4: Overview of dynamics occurring below the ball including the exhausting cylinder, the connecting tubing, and the pneumatic boost converter | 50 |
| A - 5: Basic mass flow model overview | 50 |
| A - 6: Mass flow direction switch..... | 51 |
| A - 7: Calculation of mass flow through an orifice | 51 |
| A - 8: Ideal gas law calculation of temperature..... | 52 |
| A - 9: Sample calculation for the rate of pressure change given multiple mass flows and integrated to obtain pressure in a volume | 53 |
| A - 10: Check valve dynamics at the device outlet | 54 |
| C - 1: Pneumatic boost converter prototype technical drawing | 61 |
| C - 2: Pneumatic boost converter 3D SolidWorks model | 62 |
| C - 3: Pneumatic boost converter adjuster technical drawing | 63 |
| C - 4: Adjuster 3D SolidWorks model | 64 |
| D - 1: National Instruments data acquisition card pinout | 65 |
| D - 2: Kulite ETL-375 pressure sensor data sheet | 66 |
| D - 3: Festo SPTW pressure sensor data sheet | 67 |

LIST OF TABLES

| Table | Page |
|---|------|
| 1 - 1: Annual fluid power consumption in the United States | 1 |
| 2 - 1: Equivalent components of the converter systems | 14 |
| 3 - 1: Equivalent components of the electrical and pneumatic boost converters | 26 |
| 3 - 2: Pneumatic boost converter model parameters | 36 |
| 3 - 3: Comparison of simulated and experimental tank pressure changes | 44 |

CHAPTER I. OVERVIEW

Introduction and Motivation

In the United States, fluid power accounts for between 2.0 and 2.9 Quadrillion British Thermal Units (Quads) of energy consumption per year. The total annual energy consumption in the United States is roughly 100 Quads, meaning that fluid power accounts for approximately 2% of all energy consumed in the United States. This fluid power is often very inefficient, averaging just 22% across all industries [1]. Improvements in fluid power energy efficiency are crucial in order to keep up with growing energy demands [2]. These fluid power systems are ubiquitous, but a significant portion of the total energy consumption can be attributed to industrial applications. In an industrial setting, fluid power is essential for actuation, but many of these applications utilize technologies that have not experienced substantial innovation since the 1970s. As a result, fluid power actuation is generally an extremely inefficient process. Estimated averages for the annual consumption of fluid power can be seen in the table below.

Table 1 - 1: Annual fluid power consumption in the United States [1]

| | Total Consumption (Quads/year) | Relative Consumption (% of total energy consumed in the United States) | Average Efficiency |
|-----------------------|-----------------------------------|--|-----------------------|
| Fluid Power | 2.9 | 2.9% | 22% |
| Industrial Hydraulics | 1.1 | 1.1% | 50% |
| Pneumatics | 0.5 | 0.5% | 15% |

Pneumatic systems are widely utilized for their ability to quickly and cleanly actuate systems, which translates to low costs and ease of maintenance. These qualities allowed pneumatic systems to dominate the industry at a time when energy efficiency was not a primary concern. Compressed air systems are utilized in roughly 70% of all United States manufacturing facilities, but they are the least efficient of the fluid power technologies. Unfortunately, these pneumatic systems are extraordinarily wasteful with the average industrial pneumatic system performing at an efficiency of merely 15% [1]. Energy costs have continued to increase, but pneumatic systems have seen little improvement in their energy efficiency. The poor efficiency of pneumatic actuation has led to many manufactures making the switch to electrical actuation, which has its own tradeoffs.

Some of the energy losses in pneumatic systems can be attributed to leakages, but a significant portion of the wasted energy is contained in the exhaust gas. This gas is still pressurized after actuation, but it is simply exhausted to atmosphere to prepare for the next actuation. This exhaust discharge is a source of recoverable energy that contributes to the current inefficiency of pneumatic systems. Recovering and utilizing the energy that is currently being exhausted to atmosphere could represent a significant increase

in efficiency. Even a modest increase in pneumatic efficiency would directly translate to immediate savings industry-wide.

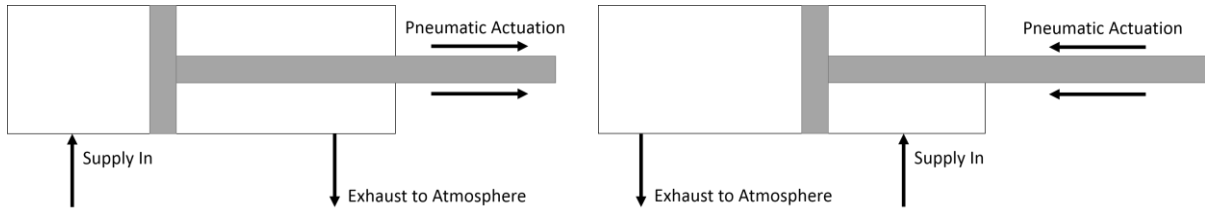


Figure 1 - 1: Pneumatic actuation and exhaust to atmosphere

Every pneumatic actuation expels exhaust gas out to atmosphere, throwing away usable energy. Both single and double-acting cylinders discharge pressurized air with every stroke. Recovering and recycling this exhaust gas energy has the potential to considerably improve the overall efficiency of these pneumatic systems. This thesis proposes a method of recovering the currently unused exhaust gas energy in a form that is immediately reusable with the goal of improved efficiency.

Literature Survey

Recovering and recycling the exhaust gas energy discharged during pneumatic actuation has been explored in the past. This literature survey will discuss methods of reusing exhaust gas and methods of increasing energy efficiency in other domains that may be relevant to pneumatics. The methodologies applied to other domains, particularly electrical and hydraulic, formed the foundation for the development of this research.

Perhaps the most straightforward method of recycling exhaust gas is the pneumatic strain energy accumulator, which is a natural rubber tube that stores the exhaust gas as strain energy. Rather than discharging the exhaust directly to atmosphere, the accumulator is attached to the exhaust port of a pneumatic actuator. When the system exhausts, the accumulator expands at constant pressure, storing the exhaust gas as strain energy [3]. The strain energy storage ability of the natural rubber provides the capacity for highly efficient energy storage [4,5]. Once stored, the accumulator can be used to power a smaller, secondary process at the exhaust pressure, which must be less than the supply pressure. Experimental results have shown these devices to be over 93% efficient [6], demonstrating an overall increase in device efficiency of 27% [7].



Figure 1 - 2: Strain energy accumulator demonstration platform [7]

Despite its ability to successfully increase pneumatic efficiency, the strain energy accumulator is only beneficial if the prerequisite conditions of its operation can be met. Specifically, there must be a secondary process (operating at a lower pressure than the supply pressure) that can be actuated by the exhaust gas stored in the accumulator. In the case of a secondary process downline from a primary process, the accumulator can potentially power this process entirely, utilizing only the exhaust from the primary process and no additional input from the supply. However, the energy in the accumulator cannot be used to power another actuation of the primary process. This restriction limits the ability of the accumulator to function as a widespread solution to pneumatic inefficiency. Ideally, the recovered energy would be universally reusable, with the ability to power primary processes at the desired supply pressure or simply reintroduce the exhaust to the supply.

For the exhaust gas energy to be reintroduced to the supply, its pressure must be increased from the exhaust pressure to the supply pressure. In the electrical domain, boost converters are commonly used to increase a voltage. The boost converters utilize a switch, a diode, and an inductor to boost the voltage dynamically. While the switch is closed, energy is stored in the inductor. When it is opened, the stored energy is forced through the diode and across a load, which sees a spike in voltage that is greater than the initial supply voltage. Applying this process to an energetically similar process in the pneumatic domain, where voltage is replaced by pressure, would achieve the desired increase in pressure that would allow the exhaust gas to be reused.

Boosting the pressure of a liquid has been accomplished in the world of hydraulics, another common source of fluid power in industrial applications. Dynamic hydraulic boosters are typically reciprocating pistons. These boosters have shown that the pressure of a liquid can be increased by utilizing the inertia

of the fluid [8,9,10][10]. Unfortunately in pneumatic applications, where the actuating fluid is air, the mass is so small that the inertia of the fluid is negligible. So an additional component is introduced to the system with an inertia to be used to transfer energy. In the pneumatic booster, a steel ball is implemented to act as the inertial component in the system as shown below.

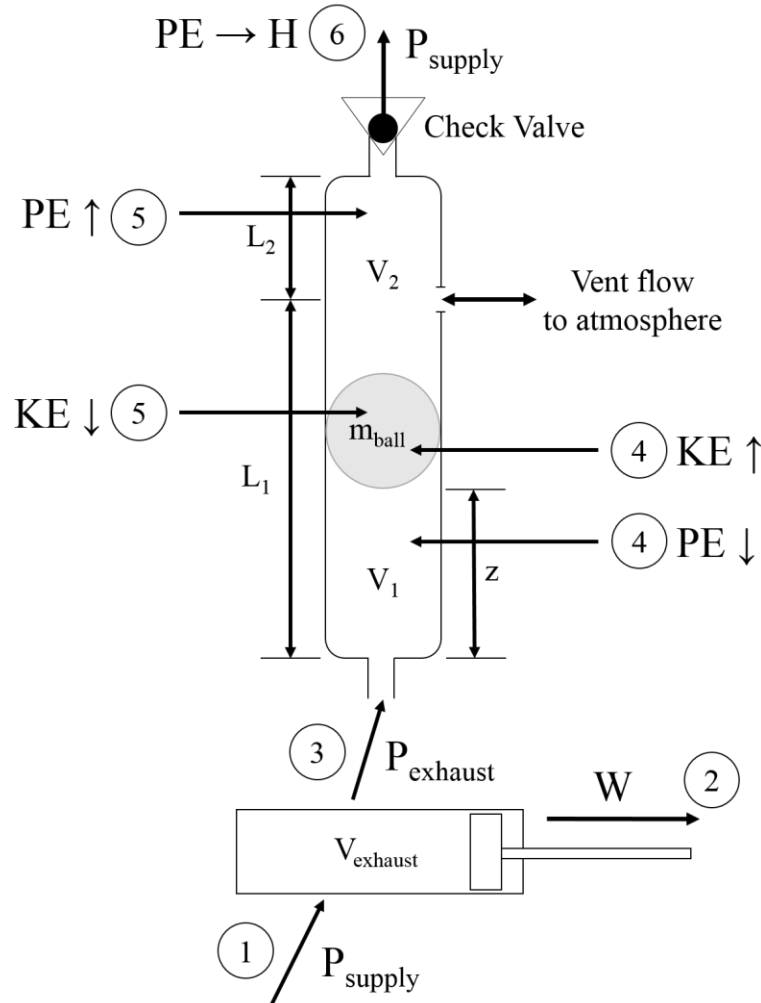


Figure 1 - 3: Pneumatic boost converter schematic

In this system, the pneumatic exhaust gas is not discharged to atmosphere but rather routed to the boost converter, which is essentially a ball in a tube with a vent and a check valve. The pressurized exhaust gas expands, forcing the ball to accelerate upwards. The vent allows the upper control volume V_2 to remain at atmospheric pressure so the ball can accelerate freely until it reaches the vent. When the ball passes the vent the upper control volume is sealed, but the inertia of the ball forces it to continue upwards, compressing and pressurizing the volume of air. When the air reaches or exceeds the supply pressure, it can escape through the check valve to be reintroduced to the supply line. This reclaimed air can then be used generically with any process that utilizes the supply.

Organization of the Document

This thesis will be presented in four chapters. The first chapter contains the introduction, motivation, and relevant literature survey. The second and third chapters present the manuscripts that detail the work completed by the author at Vanderbilt University. Chapter II presents the idea of a pneumatic boost converter in the form of a Conference Paper. This paper draws comparisons to the energetically equivalent electrical boost converter and presents a simplistic dynamic model of the system. Chapter III further develops the pneumatic boost converter: refining the model and presenting experimental validation. Lastly, Chapter IV briefly discusses the potential future directions of the pneumatic boost converter.

Manuscript 1: Dynamic Equivalence of Pneumatic and Electrical Boost Converters for Exhaust Gas Energy Reclamation

In this paper, the energetic analogy between pneumatic and electrical boost converters is explored. The concept for a physical pneumatic boost converter is presented. A simplified lossless dynamic model of the proposed system is developed and analyzed. Using this dynamic model, a boost converter design is chosen and parameters are specified to maximize the energy reclamation of the system. Analyzing the lossless model provides a theoretical upper bound of device efficiency that will drop with the introduction of losses such as friction and leakage. Manuscript 1 is based on the following conference paper:

Gibson, T. and Barth, E.J., "Dynamic Equivalence of Pneumatic and Electrical Boost Converters for Exhaust Gas Energy Reclamation," *Proceedings of the ASME/Bath 2016 Symposium on Fluid Power and Motion Control*, FPMC2016-1786, September 7-9, 2016, Bath, England UK.

Manuscript 2: Design, Model, and Experimental Validation of a Pneumatic Boost Converter

In this paper, the design of a pneumatic boost converter is presented. The device reclaims energy from the exhaust of a pneumatic actuator by drawing inspiration from a DC/DC boost converter. The design choices are discussed, and a dynamic model is developed to describe the system. A pneumatic boost converter prototype is developed and presented. Experimental results are used to validate the dynamic model and show the accuracy between the simulated and experimental results. Finally, the overall effectiveness of the device is analyzed by comparing the results of the model to the experimental results and the overall efficiency of the energy reclamation is calculated. Manuscript 2 is based on the following journal paper:

Gibson, T. and Barth, E.J., "Design, Model, and Experimental Validation of a Pneumatic Boost Converter," Submitted to the *Journal of Dynamic Systems, Measurement and Control*.

References

- [1] Love, L.J., Lanke, E., and Alles, P., 2012, "Estimating the Impact (Energy, Emissions and Economics) of the U.S. Fluid Power Industry." Oak Ridge National Laboratory, Oak Ridge, TN.

- [2] Uria-Martinez, R., O'Connor, P., and Johnson, M., 2015, "2014 Hydropower Market Report." Oak Ridge National Laboratory, Oak Ridge, TN.
- [3] Cramer, D. N. and Barth, E.J., "Pneumatic Strain Energy Accumulators for Exhaust Gas Recycling," *Proceedings of the ASME/Bath 2013 Symposium on Fluid Power and Motion Control*, FPMC2013-4488, October 6-9, 2013, Sarasota, Florida USA.
- [4] Pedchenko, A. and Barth, E.J., "Design and Validation of a High Energy Density Elastic Accumulator Using Polyurethane," *Proceedings of the ASME 2009 Dynamic Systems and Control Conference*, pp. 283-290, October 12-14, 2009, Hollywood, California USA.
- [5] Cummins, J.J., Pedchenko, A., Barth, E.J., and Adams, D.E., "Advanced Strain Energy Accumulator: Materials, Modeling and Manufacturing." *Proceedings of the ASME/Bath 2014 Symposium on Fluid Power and Motion Control*, FPMC2014-7840, September 10-12, 2014, Bath, England UK.
- [6] Cummins, J.J., Thomas, S., Nash, C., Mahadevan, S., Barth, E.J., and Adams, D.E., "Experimental Evaluation of the Efficiency of a Pneumatic Strain Energy Accumulator," *International Journal of Fluid Power*, In Review.
- [7] Cummins, J.J., Barth, E.J., and Adams, D.E., "Modeling of a Pneumatic Strain Energy Accumulator for Variable System Configurations With Quantified Projections of Energy Efficiency Increases," *Proceedings of the ASME/Bath 2015 Symposium on Fluid Power and Motion Control*, FPMC2015-9605, October 12-14, 2015, Chicago, Illinois USA.
- [8] Suzuki, K., "Application of a New Pressure Intensifier Using Oil Hammer to Pressure Control of a Hydraulic Cylinder," *J. Dyn. Sys., Meas., Control* 111(2), pp. 322-228, June 1, 1989.
- [9] Pan, M., Robertson, J., Johnston, N., Plummer, A., and Hillis, A., "Experimental Investigation of a Switched Inertance Hydraulic System," *Proceedings of the ASME/Bath 2014 Symposium on Fluid Power and Motion Control*, FPMC2014-7829, September 10-12, 2014, Bath, England UK.
- [10] Pan, M., Johnston, N., Robertson, J., Plummer, A., Hillis, A., and Yang, H., "Experimental Investigation of a Switched Inertance Hydraulic System With a High-Speed Rotary Valve," *J. Dyn. Sys., Meas., Control* 137(12), September 14, 2015.

**CHAPTER II. MANUSCRIPT 1: DYNAMIC EQUIVALENCE OF PNEUMATIC AND ELECTRICAL
BOOST CONVERTERS FOR EXHAUST GAS ENERGY RECLAMATION**

Tyler Gibson and Eric J. Barth

Vanderbilt University
Nashville, TN

Published as a Conference Paper at the
Proceedings of the Symposium on Fluid Power and Motion Control
ASME/Bath 2016

Abstract

Significant usable energy is discarded as exhaust gas in most pneumatic processes. The ability to recycle this energy could lead to significant improvements in system efficiency. This paper presents a method of dynamically converting the exhaust gas energy of pneumatic systems to a higher pressure so that it may be reintroduced to the pressure supply and reused, boosting energy efficiency of industrial pneumatic systems. This is the pneumatic equivalent of a boost converter, an electrical system that supplies a greater voltage to a load than the power source can supply. Each component of the electrical system can be analogized to an equivalent pneumatic component. The most apparent of these comparisons is the method of storing and transforming energy. In the electrical system, the energy is stored in an inductor which is charged in a closed loop. In the pneumatic system, energy can be stored as momentum. When this stored energy is discharged, a spike in voltage or pressure will be observed in the electrical or pneumatic system, respectively. Similarly, every component of the electrical boost converter can be linked to a pneumatic counterpart. With these relationships fully understood, a device to perform the pneumatic boost conversion is modeled. Successful realization of this result will confirm the analogy between the electrical and pneumatic systems, which will allow for the development of more complex pneumatic systems based on various well understood electrical converters. This paper presents simulations of both electrical and pneumatic boost converters. Insights regarding the energy conversion and its efficiency are drawn from the pneumatic model as well as from the dynamically similar electrical model.

Nomenclature

| | |
|-------------|---|
| A | Cross sectional area of ball and tube |
| A_{check} | Cross sectional area of the check valve |
| c_d | Discharge coefficient |
| c_p | Heat capacity at constant pressure |
| C | Capacitance |
| D | Diameter of ball and inner diameter of tube |
| E_C | Energy stored in the capacitor |
| E_I | Energy stored in the inductor |
| E_V | Energy stored in a control volume V |
| g | Acceleration due to gravity |
| H | Enthalpy reclaimed through the check valve |
| I_L | Current through the inductor |
| L | Inductance |

| | |
|---------------|---|
| L_1 | Length from bottom of tube to vent |
| L_2 | Length from vent to top of tube |
| m_{ball} | Mass of the ball |
| P_1 | Pressure of the lower control volume |
| P_2 | Pressure of the upper control volume |
| P_{atm} | Atmospheric pressure |
| $P_{exhaust}$ | Pressure of exhaust gas supplied to the converter |
| P_{repo} | Pressure of the gas being recycled |
| P_s | Supply pressure |
| R | Resistance |
| R_{air} | Specific gas constant of air |
| T | Temperature |
| v_0 | Voltage across the load |
| v_d | Supply voltage |
| V_1 | Volume of air beneath the ball |
| V_2 | Volume of air above the ball |
| $V_{exhaust}$ | Volume of air exhausted to the converter |
| V_{tube} | Total volume of air in the tube |
| z | Height of the ball |
| γ | Heat capacity ratio of air |

Introduction

Energy efficiency in industrial applications is currently a point of significant economic loss worldwide. According to a 2012 Department of Energy report, the United States' total energy consumption is roughly 100 Quadrillion British Thermal Units (Quads) per year. About 30% of this energy can be attributed to industrial applications, and fluid power systems account for at least 2% of the total energy consumed. The average efficiency across all hydraulic and pneumatic fluid power systems is 22%. Pneumatic equipment accounts for about 25% of the total fluid power energy consumed. Using the national average for industrial energy rates of 6.84 c/kWh, roughly \$10B is spent powering pneumatic processes each year. The average efficiency for pneumatic applications is just 15%. These inefficiencies indicate a potential for significant energy savings. A modest efficiency increase of 10% would correspond to annual savings of \$1B [1].

In pneumatic actuation, a large amount of energy is discharged as exhaust gas. The exhaust gas of a pneumatic actuator is still pressurized, storing energy, but the pressure is lower than the actuator's

operating pressure. A pneumatic strain energy accumulator has been developed to store the still-pressurized exhaust gas. The accumulator stores the exhaust gas, and its energy can be used to power a secondary process [2]. However, this method is limited by the pressure of the exhaust gas. The exhaust gas stored in the accumulator can only be used to power a process at a pressure below the original actuator's operating pressure. It cannot be reintroduced to the air supply or used to power the same actuator from which it was exhausted.

In order to reuse the exhaust energy in the actuator from which it was exhausted more generally, the air must be re-pressurized to the operating pressure. Reclaiming and recycling this energy could be a simple, cost-effective way to increase the energy efficiency of existing pneumatic systems. The Pneumatic Boost Converter proposes a method of utilizing the energy stored in the exhaust gas to pressurize a volume of air to the operating pressure of the actuator and reintroduce it to the system's air supply. Since the exhaust gas is typically discarded, any recoverable energy that it provides correlates to a direct improvement in system efficiency.

Inspiration for the Pneumatic Boost Converter is drawn from an electrical boost converter. Electrical boost converters are commonly used to obtain a voltage across a load that is greater than the supply voltage. Similarly, the Pneumatic Boost Converter aims to obtain a volume of air at a pressure that is greater than the supply pressure. These parallels in purpose motivated the design of the Pneumatic Boost Converter.

Electrical Boost Converter

The Pneumatic Boost Converter was designed to be energetically equivalent to an electrical boost converter, shown in Figure 2 - 1. The electrical boost converter consists of a supply voltage, an inductor, a switch, a diode, and a load (typically a resistor and capacitor in parallel) [3].

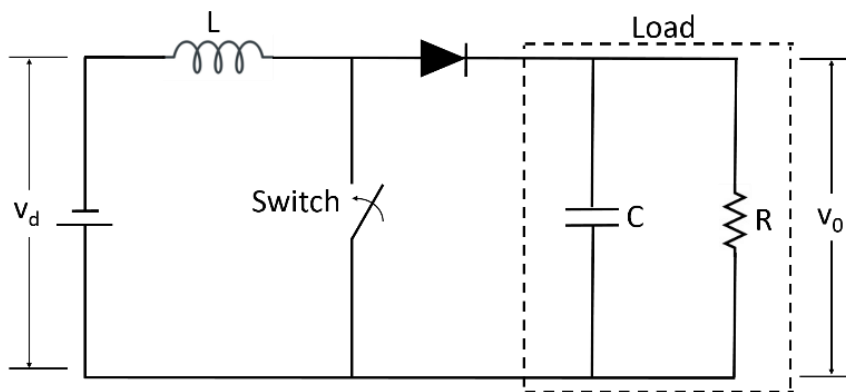


Figure 2 - 1: Circuit diagram of an electrical boost converter

When the switch is closed, the current follows the path of least resistance through the switch and charges the inductor. There is no current flowing through the diode. In this state, the voltage and current of the system are described by the following equations.

$$I_L = \frac{1}{L} \int v_d \quad (1)$$

$$v_o = \frac{-1}{RC} \int v_o \quad (2)$$

When the switch is opened, the current and the energy stored in the inductor are forced through the diode and across the load. This results in a voltage spike that is significantly higher than the supply voltage. For a load assumed to be a resistor and capacitor in parallel, the following equations describe the voltage and current of the system.

$$I_L = \frac{1}{L} \int (v_d - v_o) \quad (3)$$

$$v_o = \frac{-1}{RC} \int v_o + \frac{1}{C} \int I_L \quad (4)$$

Relevant voltage and current values can be monitored and plotted by creating a model in Simulink implementing these equations. The switch is operated with a duty cycle of 10% and a period of 0.01 seconds. The circuit is given a constant supply voltage of 12 V and resistor, capacitor, and inductor values of 1 Ω , 376 μF , and 4.1 μH respectively. The following plot shows the voltage across the load spiking when the switch opens.

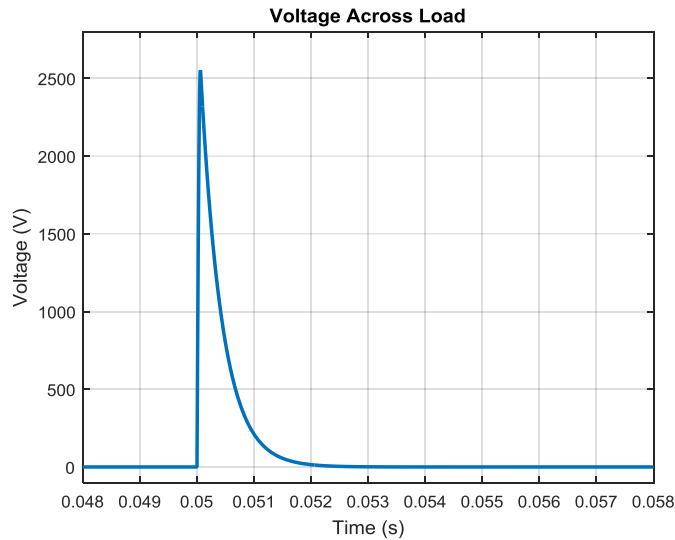


Figure 2 - 2: Voltage across the load when the boost converter switch is opened. The supply voltage is 12V.

The charging and discharging of the inductor can be seen in the plot of the current across the inductor. While the switch is closed, the current steadily increases. When the switch is opened, the current rapidly

drops to zero as it is discharged across the load. The current remains at zero until the switch is closed again.

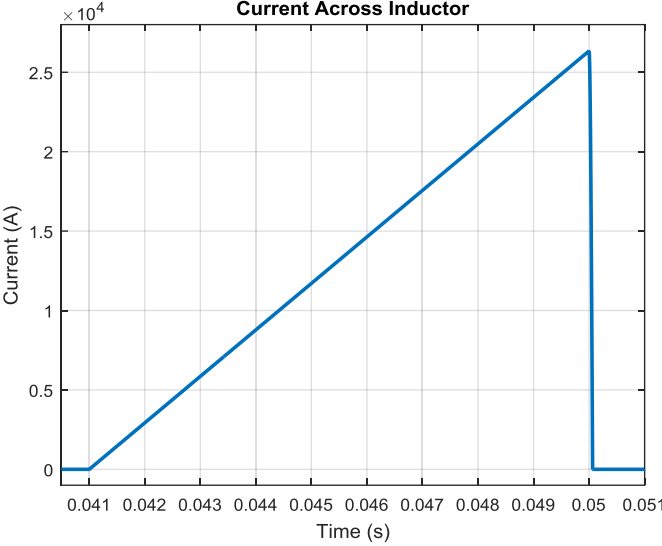


Figure 2 - 3: Current in inductor charging while the switch is closed and discharging when the switch is opened at t=0.05s

This information also allows us to obtain an energy exchange diagram, illustrating the transfer of energy between the inductor and the capacitor in the load when the switch is opened. The energy stored in the inductor and capacitor are given by the following equations.

$$E_l = \frac{1}{2} LI^2 \tag{5}$$

$$E_c = \frac{1}{2} Cv^2 \tag{6}$$

The energy exchange shows the charging of the inductor and the discharge across the capacitor when the switch is opened. The energy in the capacitor then quickly dissipates before the switch is closed, restarting the process.

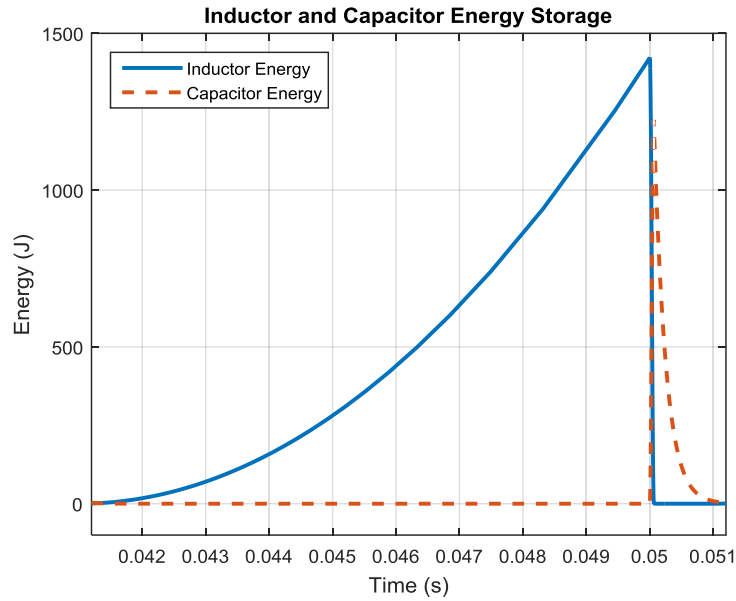


Figure 2 - 4: Energy exchange between the inductor and capacitor showing the charging of the inductor and discharge across the load

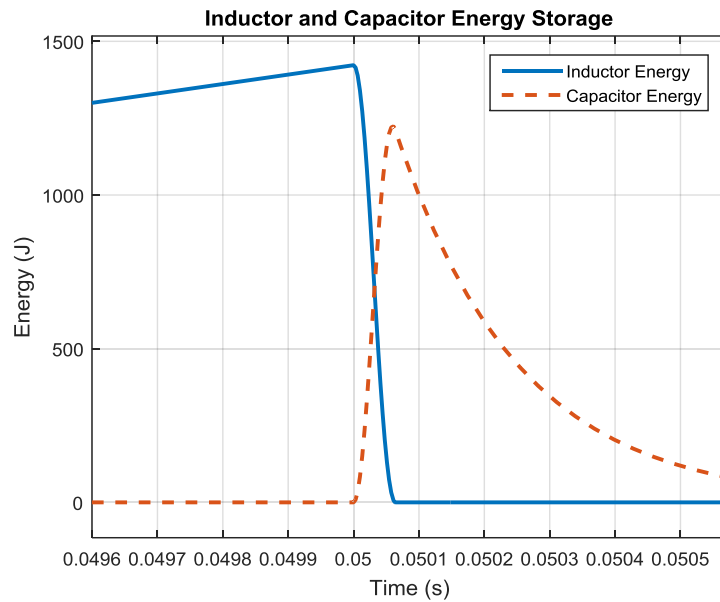


Figure 2 - 5: Zoom plot of energy exchange occurring when the switch is opened

This is the basis of an electrical boost converter that served as the foundation for the development of the Pneumatic Boost Converter. To translate these results to a pneumatic system, it is important to first understand the energetically equivalent components between the two systems.

Table 2 - 1: Equivalent components of the converter systems

| Electrical Converter | Pneumatic Converter |
|-----------------------------|----------------------------|
| Supply Voltage | Exhaust Gas Pressure |
| Inductor | Momentum |
| Diode | Check Valve |
| Load Voltage | Reclaimed Gas Pressure |
| Switch | Vent |

Pneumatic Boost Converter

The equivalent proposed system is composed of an upright rigid tube containing a spherical ball, dividing the tube into two fluctuating control volumes. The system utilizes the pressurized exhaust air as an input, and the energy recovered at the supply pressure is the output. This system would be easily implementable, as it can be directly attached to any existing pneumatic system. Simply connect any exhaust port to the tube's input, and the output can be reintroduced directly to the supply line. The Pneumatic Boost Converter can be seen below.

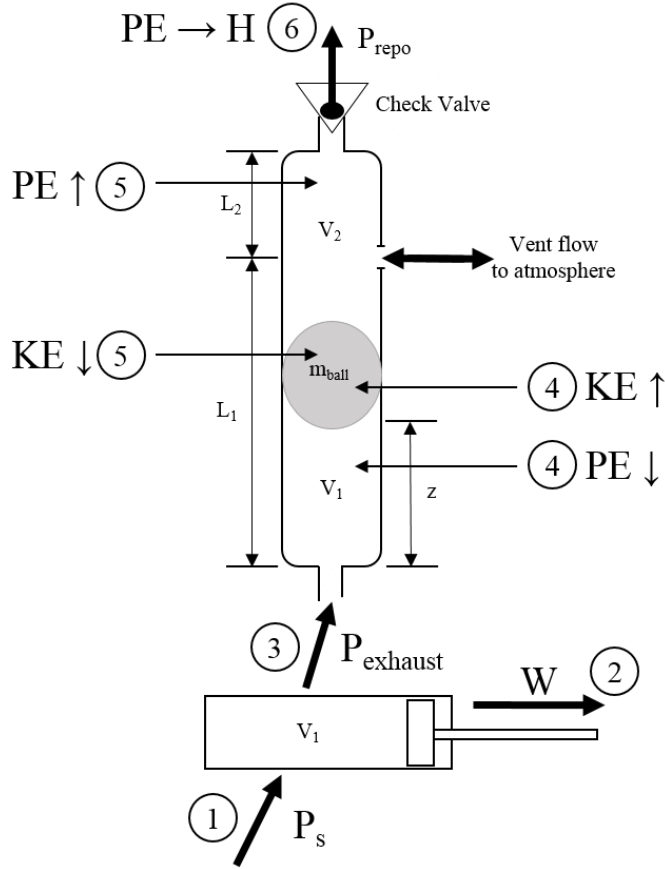


Figure 2 - 6: Diagram of proposed Pneumatic Boost Converter

The sequence shown in Figure 2 - 6 indicates the flow of energy in numerical order. The process begins with a pneumatic actuation at the operating pressure of P_s ①, and the actuator does work ②. The control volume V_2 is initially at atmospheric pressure when the still pressurized exhaust gas is fed to the Pneumatic Boost Converter. This is accomplished by connecting the exhaust port of the actuator's valve to the input of the tube ③. The pressure differential across the ball causes V_1 (which also includes the piston cylinder volume) to expand and the ball to gain velocity. While the ball is beneath the vent, V_2 vents to atmosphere and the ball accelerates freely. In this stage, the potential pressure energy of V_1 is transferred to the kinetic energy of the ball ④. When the ball passes the vent, V_2 is compressed. During this stage, the kinetic energy of the ball is transferred to the potential pressure energy of V_2 ⑤. When the pressure of V_2 surpasses the supply pressure, the potential energy escapes through the check valve as enthalpy H ⑥.

To properly design and implement the system, a model is needed to fully understand its dynamics. Understanding the flow of energy throughout the process will allow us to make design decisions that will maximize the efficiency of the system. Firstly, the acceleration of the ball can be described by:

$$\ddot{z} = -g - \frac{A}{m_{ball}}(P_2 - P_1) \quad (7)$$

The velocity and position of the ball can then be solved for by integration. The velocity and position can be used to determine the two control volumes and their rates of change.

$$V_1 = Az + V_{exhaust} \quad (8)$$

$$\dot{V}_1 = A\dot{z} \quad (9)$$

$$V_2 = V_{tube} - Az \quad (10)$$

$$\dot{V}_2 = -A\dot{z} \quad (11)$$

The pressure of a control volume was calculated by integrating the following equation for rate of change of pressure, where γ and c_p are the constant properties of air.

$$\dot{P} = \frac{(\gamma - 1)\dot{m}c_p T - \gamma P \dot{V}}{V} \quad (12)$$

Solving this equation for either control volume requires the mass flow rate into or out of the control volume and the temperature of the flow. The temperature was calculated using the ideal gas law, where R is the specific gas constant of air.

$$T = \frac{PV}{mR_{air}} \quad (13)$$

The mass flow rate was calculated following the methodology described in [4] using the upstream and downstream pressures, the temperature of the flow, and the orifice area. The lower control volume only experiences mass flow through the vent and only after the ball has passed the vent (when $z > L_1 - D/2$). The upper control volume experiences mass flow through the check valve but only in the negative direction (leaving the control volume) when $P_2 > P_{reps}$. The upper control volume can also have a mass flow through the vent when the ball is beneath it (when $z < L_1 - D/2$). Integrating the mass flow rates allows the model to track the total mass of air in each control volume.

Modeling Results

With the system dynamics modelled in Simulink, the Pneumatic Boost Converter was compared to the electrical converter to verify the equivalencies drawn between the two systems. The first noteworthy comparison is between the voltage across the load and the pressure of the upper control volume. The pressure of the upper volume can be seen in Figure 2 - 7.

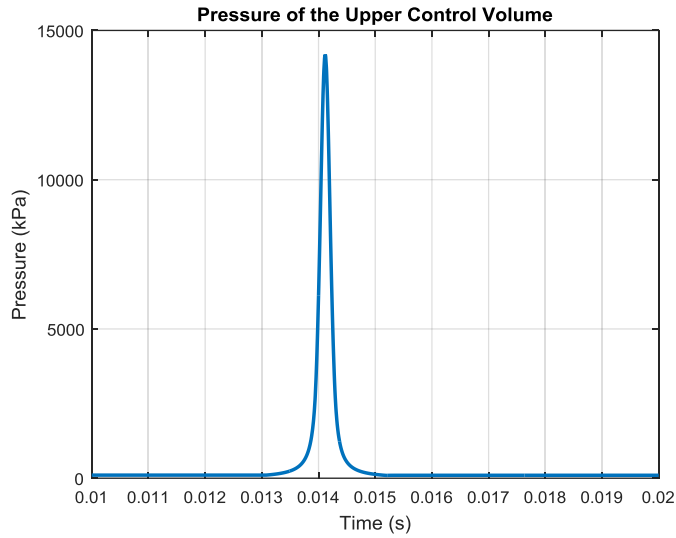


Figure 2 - 7: The pressure spike experienced in V_2 when the ball passes the vent, sealing it

Comparing to the load voltage of the electrical boost converter shown in Figure 2 - 2, we can see a similar behavior. The pressure begins at atmosphere and quickly increases when the vent is sealed similar to when the switch is opened in the electrical boost converter. In the pneumatic converter, the curve is smoother, as the transfer of energy from the pressurized exhaust gas to the ball to the pressure of the upper volume is not instantaneous like the switching of a circuit. When the vent is opened, the pressure rapidly returns to atmospheric pressure. In the Pneumatic Boost Converter, this energy is transferred to the momentum of the ball, gaining an upward velocity through the tube. The momentum of the ball is proportional to its velocity which can be seen in Figure 2 - 8.

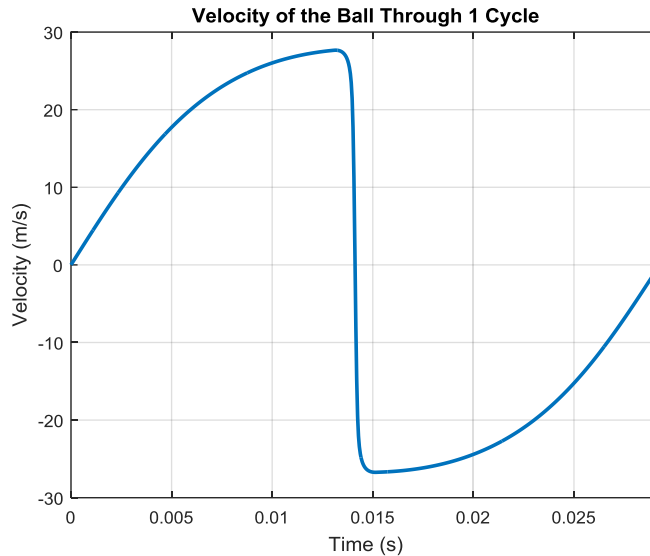


Figure 2 - 8: The velocity of the ball \dot{z} through one energy exchange cycle

These results can be compared to the current in the inductor shown in Figure 2 - 3. Similar to the pressure plot, the movement of the ball is not instantaneous like the switching of the circuit, but the plot shows the same trend. The ball starts at rest then as the lower control volume expands, the velocity of the ball rapidly increases. When the ball passes the vent, sealing the upper control volume, the velocity rapidly returns to zero. This is very similar to the manner in which the current increases in the inductor until the switch is opened, when it discharges to zero. The primary difference seen in the velocity plot is that the ball can obtain a negative velocity, while the current through the inductor stops at 0. This implies a kinetic energy in the ball, the effects of which will be discussed later in the paper.

The results shown in these plots utilize a ball and tube geometry selected based on feasibility and ease of implementation. The inner diameter of the tube was chosen to be 0.5" (12.7 mm). The volume of the exhaust gas discharge was selected to be a common piston size, 6" (152.4 mm) in length by 9/16" (14.3 mm) in diameter. The pressures used for the exhaust gas and supply were chosen to be commonly seen pressures, 40 psi (275.8 kPa) and 80 psi (551.6 kPa) respectively. To determine the appropriate tube length and vent position, the model simulation was run with varying combinations, recording the reclaimed energy in each case. The plot below shows the energy reclaimed for a system with L_1 varying from 125 mm to 350 mm and L_2 varying from 25 mm to 35 mm. Considering the physical limitations of the system, a combination of L_1 and L_2 can be selected to reclaim the maximum amount of energy.

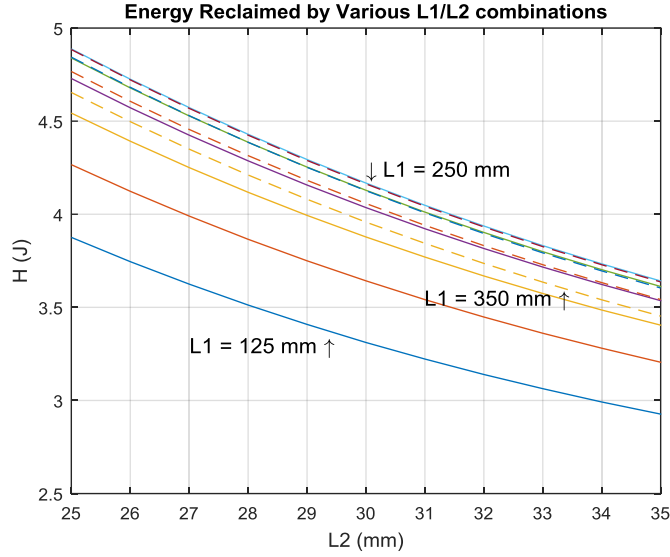


Figure 2 - 9: Maximum energy reclaimed by various combinations of tube lengths

For the model, L_2 was selected to be 30 mm, just over double the diameter of the ball. To maximize the energy reclamation with this L_2 , L_1 was chosen to be 250 mm, based on the results of Figure 2 - 9. With these values, the energy exchange between the two control volumes, the ball, and the energy leaving through the check valve can be acquired.

The total potential energy in a volume of pressurized air is calculated with the expression:

$$E_V = PV^\gamma \frac{V_f^{1-\gamma} - V^{1-\gamma}}{1-\gamma} \quad (14)$$

Where the final volume V_f is given by:

$$V_f = \left(\frac{P}{P_{atm}} \right)^{1/\gamma} V \quad (15)$$

The energy of the ball is simply the sum of its kinetic and potential gravitational energy.

$$E_{ball} = \frac{1}{2} m_{ball} \dot{z}^2 + m_{ball} g z \quad (16)$$

The gravitational energy of the ball is negligible when compared to its kinetic component. This term can be compared to Equation (5), which describes the energy of the inductor. The two equations are in the same form, and both are dependent on flow (velocity and current). The energy reclaimed through the check valve is obtained by integrating the following expressions where \dot{m} is the rate of flow through the check valve.

$$\dot{H} = \dot{m} c_p T_{flow} \quad (17)$$

$$\dot{m} = A_{check} c_d \Psi(P_s, P_2) \quad \text{for } P_2 > P_s \quad (18)$$

Where Ψ is a function dependent on the supply pressure and pressure of V_2 whose functional form is specified in [4].

These equations provide four energies that can be tracked throughout the model simulation (the upper and lower control volumes are calculated separately). The exchange between them can be seen in the plot below.

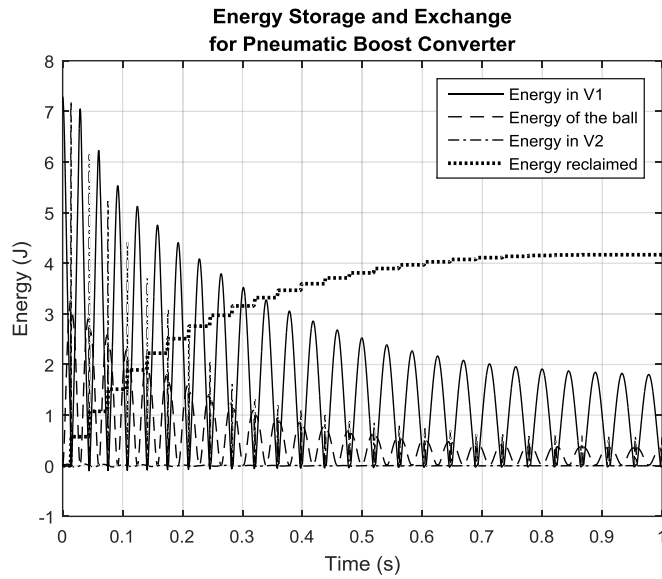


Figure 2 - 10: Pneumatic energy exchange between the two potential pressure energies, the kinetic energy of the ball, and the energy being reclaimed through the check valve

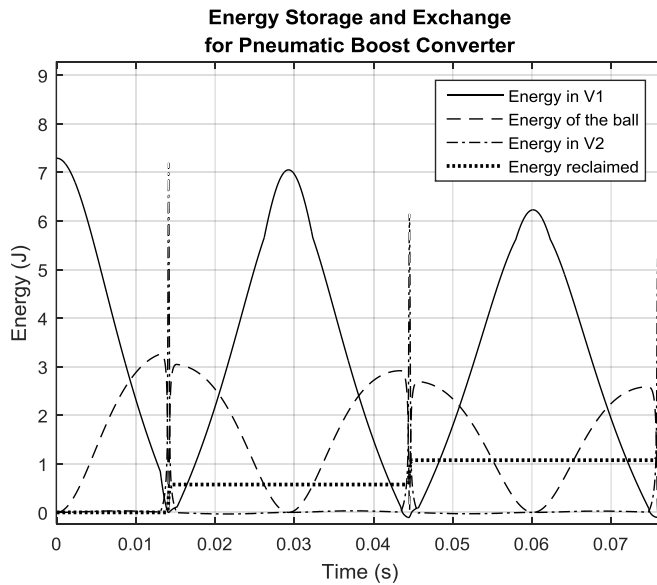


Figure 2 - 11: Zoomed view of the first three cycles of the pneumatic energy exchange

Figure 2 - 11 shows that the initial volume of pressurized exhaust gas is storing 7.3 J of energy. This is the total energy that is typically discarded when the exhaust gas is expelled to atmosphere. Once the ball has stopped moving, the total energy reclaimed through the check valve is about 4.2 J. This energy can be

reintroduced directly into the supply line, making it effectively free energy. These results represent a 57.16% efficiency in energy reclamation from the exhaust gas.

As seen in Figure 2 - 10, the energy reclamation is not completed in a single shot. The ball compresses V_2 extremely quickly causing a huge spike in P_2 , while P_1 is rapidly venting to atmosphere. Some of the potential pressure energy of V_2 is reclaimed through the check valve. The large pressure differential across the ball in the opposite direction then launches the ball downwards with a negative velocity shown in Figure 2 - 8. The momentum of the ball compresses V_1 , while V_2 vents to atmosphere. This causes another pressure differential launching the ball upward again, compressing V_2 and forcing some re-pressurized air through the check valve, increasing the energy reclaimed. This process repeats several times. As energy leaves the system, each cycle operates at a lesser pressure differential, and less energy is reclaimed through the check valve.

This results in the ball “bouncing” along the tube, with the vent as its switching point. This is akin to the duty-cycle switching of the electrical boost converter. The primary difference is that the switching of the Pneumatic Boost Converter is state-dependent rather than actively controlled.

Conclusions and Future Work

The proposed Pneumatic Boost Converter is a simple passive device that recovers energy from exhaust gas that is typically thrown away. Energetic equivalence to the commonly used electrical boost converter allows for parallels to be drawn between the systems. The energetically equivalent components described in Table 1 inspired the design of the Pneumatic Boost Converter. The model developed to describe the system allowed the properties of the converter to be carefully selected, and the results of the simulations show that the system could reclaim up to 57.16% of the energy typically exhausted.

It must be noted that this model is fairly idealized, and some assumptions have been made. The model does not account for losses due to the friction between the ball and the tube. It does not account for leakage around the ball from V_1 to V_2 or vice-versa. The model equations assume that the control volumes expand and contract adiabatically.

These unmodelled losses will be incorporated into future models. For now, this idealized model serves its intended purpose of demonstrating the energetic equivalence between the electrical and pneumatic boost converters. This knowledge will allow the model to be updated and designed with the application of established boost converter practices by transferring them to the pneumatic domain.

Discharging exhaust gas is neglecting usable energy. Recycling this energy through the implementation of the Pneumatic Boost Converter could result in huge savings in industrial pneumatics. The Pneumatic Boost Converter does not require a secondary actuator operating at a lower pressure like other energy harvesting and recycling schemes such as the pneumatic strain energy accumulator. It does not require replacing current systems. A simple converter that could be easily attached to any existing pneumatic system would be a straightforward, no-hassle way to increase pneumatic efficiency.

This work has demonstrated the energetic analogy between the electrical and pneumatic boost converters. The electrical boost converter is a well-understood, commonly implemented system that typically operates at efficiencies of roughly 80% [5]. The efficiency achieved by the model of the Pneumatic Boost Converter is comparable, with some expected energy losses. The analogy between the electrical and pneumatic systems will allow future designs to consider the established understanding of electrical boost converters and the translation to the pneumatic domain. The dynamic similarity between the systems lets electrical boost converter principles be implemented in the pneumatic system. This knowledge could also be applied to different electrical converters, such as a buck-boost converter or Ćuk converter in future designs.

The model provides a convincing argument to proceed with the development of an experimental prototype in order to validate the model. Experimental data will help identify any unmodeled phenomena that may impact the operation of the boost converter. Updating the model to match the experimental results will then allow complete freedom to modify aspects of the design within the model and accurately depict how the changes would impact the results in the experimental prototype. This will help design the Pneumatic Boost Converter to achieve the maximum possible energy reclamation.

Acknowledgments

This work was supported by a grant from the National Fluid Power Association.

References

- [1] Love, L.J., Lanke, E., and Alles, P., 2012, "Estimating the Impact (Energy, Emissions and Economics) of the U.S. Fluid Power Industry." Oak Ridge National Laboratory, Oak Ridge, TN.
- [2] Cummins, J.J., Pedchenko, A., Barth, E., and Adams, D.E., 2014, "Advanced Strain Energy Accumulator: Materials, Modeling and Manufacturing." Proceedings of the 2014 Bath/ASME Symposium on Fluid Power and Motion Control. Sept 11. Bath, England UK.
- [3] Mohan, N., Undeland, T.M., and Robbins, W.P., 2003, *Power Electronics*, John Wiley & Sons, Inc., New Jersey.
- [4] Richer, E., and Hurmuzlu, Y., 2000, "A High Performance Pneumatic Force Actuator System: Part I—Nonlinear Mathematical Model." ASME Journal of Dynamic Systems, Measurement, and Control 122, pp. 416-425.
- [5] Eichhorn, T., 2008, "Boost Converter Efficiency Through Accurate Calculations." Power Electronics Technology, Grass Valley, CA.

**CHAPTER III. MANUSCRIPT 2: DESIGN, MODEL, AND EXPERIMENTAL VALIDATION OF A
PNEUMATIC BOOST CONVERTER**

Tyler Gibson, Eric J. Barth

Vanderbilt University
Nashville, TN

Submitted to the
ASME Journal of Dynamic Systems, Measurement and Control

Abstract

This paper presents the design and dynamic model for a prototype pneumatic boost converter, a device developed to be an energetic equivalent to the electrical boost converter. The design of the system selects pneumatic components that are energetically equivalent to the components used in the analogous system in the electrical domain. A dynamic model for the pneumatic boost converter that describes the rapidly fluctuating pressures and volumes is developed. Movement within the system and mass flow through orifices connecting control volumes are also modeled. A prototype was developed to reclaim air at 653 kPa (80 psig) and experimental data was collected at two points within the system. This experimental data is used to validate the dynamic model by comparing experimental and simulated pressures. The experimental data is also used to calculate the total energy reclaimed by the pneumatic boost converter as well as the system efficiency.

Introduction

Pneumatic power is an extremely common form of actuation in the United States, accounting for the consumption of roughly 500 trillion BTU of energy per year. It is particularly ubiquitous in industrial applications due to its speed, simplicity, and ease of maintenance. In the past, it was also very cost-efficient. However with rising energy demands and increasing competition from alternative methods of actuation, the inefficiencies of pneumatic actuation are severely limiting its cost effectiveness. A report by the Department of Energy in 2012 estimated the average efficiency of pneumatic systems to be just 15% [1]. Increasing this efficiency is essential to ensuring that pneumatic systems remain competitive, cost-effective form of actuation.

One method of improving overall plant energy efficiency that is becoming more commonplace in industrial applications is the energy audit. These audits are designed to identify predominant sources of energy inefficiency and minimize unnecessary waste [2]. Minimizing energy usage is a direct method of increasing energy efficiency and cost-effectiveness. Industrial energy audits in the pneumatic domain often include reducing the pressure used for actuations by installing local regulators and minimizing leakages in the distribution system.

The overall inefficiency of pneumatic systems can be attributed to a number of factors. Pneumatic systems always suffer from some amount of leakage, but a significant amount of energy is lost with each pneumatic actuation through the discharged exhaust gas. This exhaust gas is still pressurized after actuation, meaning that it is storing usable energy. By discharging it to atmosphere, the energy stored in the still-pressurized exhaust gas is completely lost. Exhaust gas of pneumatic systems is a source of recoverable energy that is currently neglected in pneumatic actuation. Recovering even a small amount of the energy currently lost through exhaust discharge would correlate to a substantial increase in system efficiency and consequently cost effectiveness.

Methods of recovering and recycling the exhaust gas energy have been explored by researchers in the form of a strain energy accumulator. The accumulator is made of a natural rubber that expands to store the exhaust gas as strain energy [3]. The strain energy in the accumulator is stored with high efficiency [4,5]. It is stored at a constant pressure, and once stored the exhaust gas can be reused at any time. The device is very efficient at storing and discharging the exhaust gas energy. It has experimentally demonstrated a 93% efficiency [6] and increased overall device efficiency by 27% [7].

However, the strain energy accumulator has some unavoidable limitations. Since it stores the exhaust gas at a lower pressure than the original actuation pressure, the energy in the accumulator cannot be reused to power the same process from which it was reclaimed. The reclaimed exhaust energy can be used to fully power a secondary process at the lower exhaust pressure, entirely independent of the pneumatic supply. In this specific scenario, the strain energy accumulator is very effective. It increases system efficiency, and utilizing only the energy that is already being exhausted by the primary process, it has the ability to completely power a secondary process. In the absence of this primary and secondary process setup, the strain energy accumulator is not effective. If all processes require the same supply pressure, then the reclaimed exhaust will not contain enough energy to power another process. A more general device would reclaim the exhaust energy and boost it to the supply pressure so that it is universally reusable by any process that is powered by the pneumatic supply.

In this paper, an alternative method of exhaust gas energy reclamation is presented and described. The design, dynamic model, and experimental setup of a pneumatic boost converter will be fully discussed. The presented boost converter converts the low pressure, high volume exhaust gas energy to a high pressure, low volume gas that can be directly reintroduced to the supply and generically reused for pneumatic actuation. By increasing the pressure of the reclaimed gas to the supply pressure, a specific process or configuration, such as requiring a secondary actuation at a lower pressure, is not necessary. By reclaiming and reintroducing the air to the supply, it is directly contributing to the energy requirements of the facility. Experimental data is used to validate the dynamic model, which describes the energy transfer and pressure changes within the device.

Design

The pneumatic boost converter is inspired by the electrical boost converter, a commonly used and extremely efficient device [8] used to deliver a voltage to a load that is greater than the supplied voltage. The electrical boost converter is composed of a voltage supply, an inductor, a switch, a diode, and a load as shown below [9].

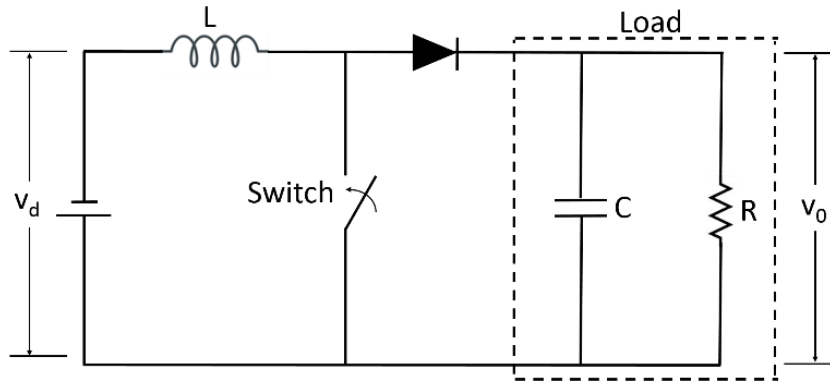


Figure 3 - 1: Circuit diagram of an electrical boost converter

When the switch is closed, the current follows the path of least resistance charging the inductor. Once charged, the switch is opened and the current is forced through the diode and across the load. The energy stored in the charged inductor in addition to the constantly supplied voltage deliver a voltage spike to the load that is greater than the supply voltage. Translating this energy transfer to an equivalent system in the pneumatic domain is the objective of the pneumatic boost converter [10].

The energetically analogous system in the pneumatic domain would generate a pressure spike that is greater than the supplied pressure. This spike in pressure is the effort needed to reclaim the exhaust gas energy. The effort and corresponding flow allows energy to flow back into the supply line. Each component in the electrical boost converter can be adapted to the pneumatic domain. The energetically equivalent pneumatic components are the exhaust gas, an inertia, a vent, a check valve, and the reclaimed gas pressure.

Table 3 - 1: Equivalent components of the electrical and pneumatic boost converters

| Electrical Converter | Pneumatic Converter |
|----------------------|------------------------|
| Supply Voltage | Exhaust Gas Pressure |
| Inductor | Inertia |
| Switch | Vent |
| Diode | Check Valve |
| Load Voltage | Reclaimed Gas Pressure |

The proposed pneumatic boost converter is an upright rigid tube containing a spherical ball. The device inlet is connected to the exhaust of a pneumatic actuator, and the outlet reintroduces the pressurized air to the pneumatic supply line. This device is generically applicable to any fast exhausting pneumatic actuation,

and the reclaimed energy is simply added to the supply where it can be universally reused. It is designed to be a simple addition to existing hardware that does not require specific actuators or configurations.

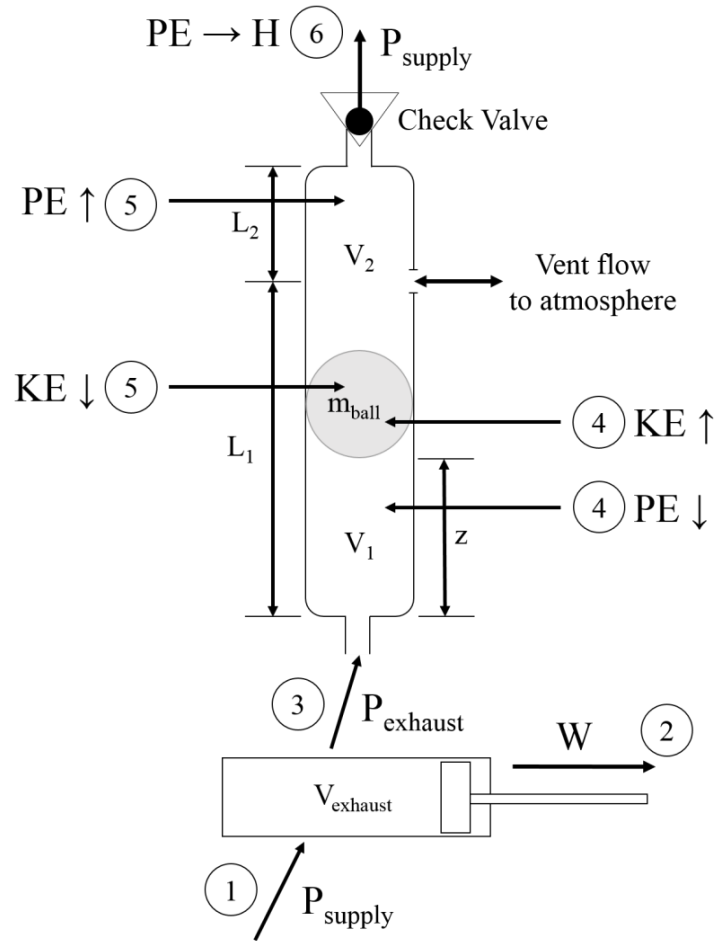


Figure 3 - 2: Pneumatic boost converter prototype schematic

The diagram above shows the transfer of energy through the pneumatic boost converter. The process begins with the supply pressure, P_{supply} , being delivered to an actuator ①, which then does work ② as normal. However rather than discharging the exhaust gas to atmosphere, it is routed to the inlet of the pneumatic boost converter ③. When the actuator exhausts, the pressurized exhaust gas expands into the pneumatic boost converter, accelerating the ball upward. Potential pressure energy is transferred to the ball and stored as kinetic energy ④, similar to the charging of the inductor in the electrical boost converter. The volume above the ball, V_2 , freely vents to atmosphere to maintain atmospheric pressure, minimize the resistance on the ball, and maximize the energy stored as kinetic energy. When the ball passes the vent, the volume above the ball is sealed but the ball's inertia causes it to continue upward. The potential pressure energy above the ball increases and the kinetic energy of the ball decreases as the upper volume is compressed ⑤. When the pressure above the ball exceeds the check valve's back pressure, P_{supply} , air escapes through the check valve where it is reintroduced to the supply ⑥. This is energetically analogous

to the electrical boost converter switch opening and forcing the current through the diode and across the load. The air reclaimed through the check valve represents the total energy recovered from a pneumatic actuation's typically discarded exhaust gas energy.

The transfer of energy through the pneumatic boost converter is illustrated by the bond graph of the system presented below. The assumption of adiabatic expansion allows the graph to be modeled using pressure and rate of volume change for the effort and flow, respectively.

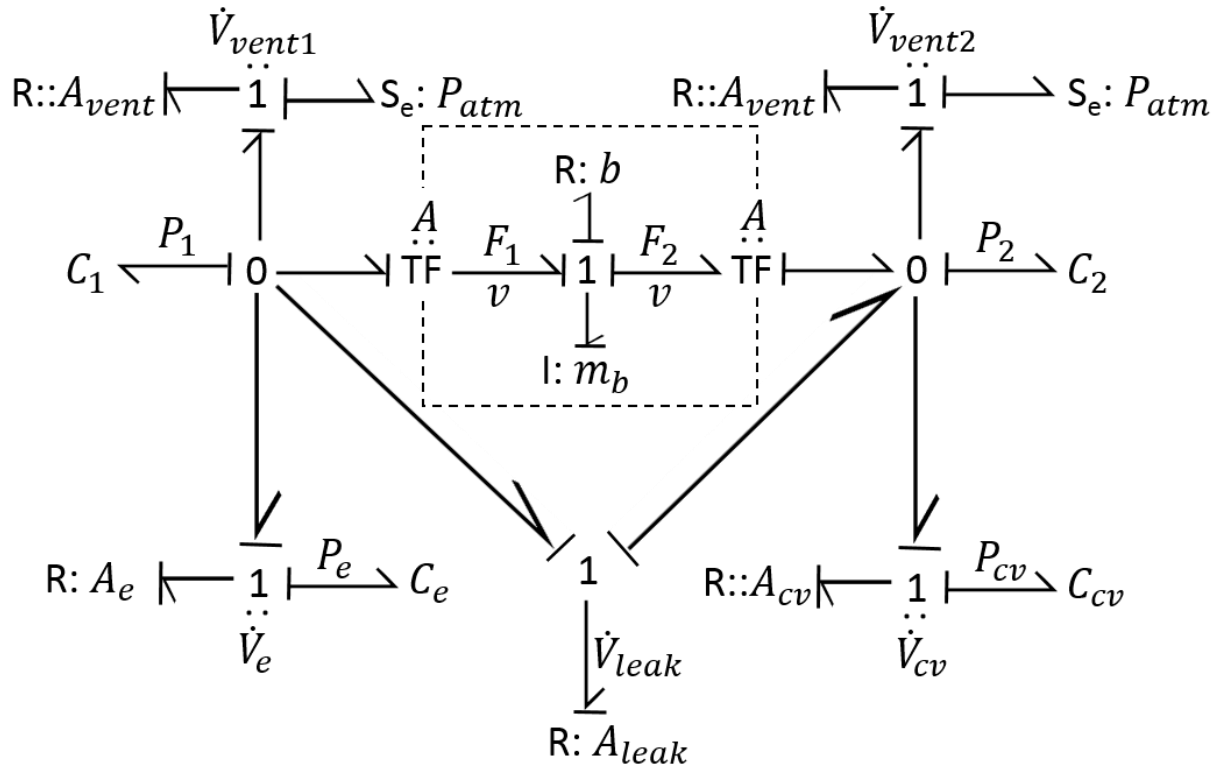


Figure 3 - 3: Pneumatic boost converter bond graph

where P is pressure, \dot{V} is volume rate of change, C is the capacitance representing the compressibility of air, A is the cross sectional area of the tube, and all A variables with a subscript denote an orifice area. The subscripts 1 and 2 denote the volume of air in the tube below and above the ball, respectively, e denotes the volume of the exhausting cylinder, cv denotes the volume beyond the check valve, and $leak$ denotes the leakage around the ball. The bond graph acts in the fluid domain, except for within the dashed line which describes the ball in the mechanical domain. It is worth noting that the area of the vent and the check valve are nonlinear relationships (denoted by the double colon). The two vent flows shown in the bond graph both describe the same physical vent, but the interaction between two separate volumes results in two different effective flows. These relationships will be further explored in the calculations for mass flow, which can be found in the subsection titled Device Description.

Dynamic Model

The dynamics of the system are largely dependent on the position of the ball as it travels through the pneumatic boost converter. The ball divides the tube into two separate control volumes, one beneath the ball and one above the ball (V_1 and V_2 respectively). A dynamic description of the forces acting on the ball served as the foundation for the dynamic model. The equation describing the dynamics of the ball is given by:

$$m\ddot{z} + b\dot{z} = A(P_1 - P_2) - mg \quad (1)$$

where m is the mass of the ball, b is the effective damping coefficient, A is the cross-sectional area of the tube, P_1 is the pressure of V_1 , P_2 is the pressure of V_2 , g is the gravitational constant, z is the vertical position of the ball, and the dot-notation indicates a time derivative. Solving for the acceleration of the ball yields the equation:

$$\ddot{z} = \frac{1}{m} [A(P_1 - P_2) - mg - b\dot{z}] \quad (2)$$

which is then integrated to obtain the velocity and position of the ball. The ball is assumed to be at rest at the bottom of the tube ($z = 0$) at the beginning of each actuation. The position of the ball is used to calculate the control volumes V_1 and V_2 by multiplying by the cross-sectional area.

$$V_1 = Az + V_{exhaust} \quad (3)$$

$$\dot{V}_1 = A\dot{z} \quad (4)$$

$$V_2 = V_{tube} - Az \quad (5)$$

$$\dot{V}_2 = -A\dot{z} \quad (6)$$

The model accounts for the dead volume surrounding the ball, as well as the dead volume at the top and bottom of the tube with initial conditions given by the constants $V_{exhaust}$ and V_{tube} . $V_{exhaust}$ indicates the volume of the piston chamber being exhausted in addition to any dead volume in the valve, tubing, or boost converter itself. V_{tube} indicates the volume in the device above the ball as well as the dead volume surrounding the ball and check valve at the top of the tube. These equations describe the motion of the ball through the pneumatic boost converter as a function of the pressure on either side of the ball. These pressures fluctuate rapidly with the changing volumes, masses, and temperatures of the system.

A. Pressure Dynamics

The pressure in both control volumes is calculated by integrating the following equation for the rate of change of pressure:

$$\dot{p} = \frac{(\gamma - 1)\dot{m}c_p T_{flow} - \gamma P\dot{V}}{V} \quad (7)$$

where γ and c_p are the constant heat capacity properties of air. This equation assumes adiabatic expansion and compression due to the speed of the process. All volumes initiate at atmospheric pressure except for the discharging exhaust volume. The volume and volumetric rate of change are obtained from the ball

dynamics as given by Equations 3 - 6. The mass flow rate, \dot{m} , will be discussed in the following subsection. The temperature of the mass flow, T_{flow} , is calculated using the ideal gas law where:

$$T = \frac{PV}{mR_{air}} \quad (8)$$

The pressure and temperature in the control volumes is dependent on the compression or expansion of the control volume as well as the air flowing into or out of the volume. All temperatures initiate at room temperature. Air flows between several sections quickly and continuously. The rate of flow for these air masses as well as their temperatures are a significant factor in the dynamic motion and pressure within the pneumatic boost converter.

B. Mass Flow

The mass flow rate into and out of the control volumes is essential to dynamically model the system's pressures, volumes, and temperatures. The relevant mass flows are into the lower control volume from the exhausting cylinder, through the vent from either V_1 or V_2 depending on the ball position, through the check valve, and between the control volumes as leakage around the ball. All were modeled using the equations for mass flow through an orifice determined by Richer and Hurmuzlu [11].

$$\dot{m} = \begin{cases} C_d A_v C_1 \frac{P_u}{\sqrt{T}} & \text{if } \frac{P_d}{P_u} \leq P_{cr} \\ C_d A_v C_2 \frac{P_u}{\sqrt{T}} \left(\frac{P_d}{P_u}\right)^{1/\gamma} \sqrt{1 - \left(\frac{P_d}{P_u}\right)^{(\gamma-1)/\gamma}} & \text{if } \frac{P_d}{P_u} > P_{cr} \end{cases} \quad (9)$$

where \dot{m} is the mass flow through the valve orifice, C_d is the discharge coefficient, A_v is the orifice area, T is the flow temperature, P_u is the upstream pressure, P_d is the downstream pressure, and C_1 , C_2 , and P_{cr} are described by:

$$C_1 = \sqrt{\frac{\gamma}{R} \left(\frac{2}{\gamma+1}\right)^{(\gamma+1)/(\gamma-1)}} \quad (10)$$

$$C_2 = \sqrt{\frac{2\gamma}{R(\gamma-1)}} \quad (11)$$

$$P_{cr} = \left(\frac{2}{\gamma+1}\right)^{\gamma/(\gamma-1)} \quad (12)$$

where γ and R are the heat capacity ratio and individual gas constant of air, respectively. The effective orifice area A_v is calculated using the given flow coefficient for the valves used. The flow coefficient is described as the volumetric flow rate of water at 60°F through a valve with a pressure differential of 1 psi in the units of US gallons per minute. In standard units, the flow coefficient C_v can be used to calculate the effective orifice area using the equation:

$$A_v = \frac{C_v}{\sqrt{\frac{2}{\rho}(P_1 - P_2)}} \quad (13)$$

The only mass flow rate that is not calculated using Equation 13 to determine the effective orifice area is the leakage of air around the ball between V_1 and V_2 . This area is calculated using the given tolerances for the pneumatic boost converter ball and tube. The annular flow around the ball is assumed to be comparable to the flow through an orifice valve of the same area and sufficiently described by Equations 9 - 12.

These equations are used to calculate the mass flow rates within the system, which are then integrated to obtain the mass of air in each section. The initial condition for the mass of each section is calculated with the ideal mass law such that:

$$m_{air} = \frac{PV}{R_{air}T} \quad (14)$$

C. Device Description

The generic equations for the mass flow rates and pressure dynamics given in the sections above can be applied to the system to obtain pressure equations for each of the control volumes in the pneumatic boost converter. The pressure dynamics of the two primary control volumes V_1 and V_2 are described by the following equations:

$$\dot{P}_1 = \frac{(\gamma - 1)c_p(\dot{m}_{exhaust}T_{flowexh} + \dot{m}_{vent1}T_{flowvent} + \dot{m}_{leak}T_{flowleak}) - \gamma P_1 \dot{V}_1}{V_1} \quad (15)$$

$$\dot{P}_2 = \frac{(\gamma - 1)c_p(\dot{m}_{vent2}T_{flowvent} - \dot{m}_{leak}T_{flowleak} + \dot{m}_{cv}T_{flowcv}) - \gamma P_2 \dot{V}_2}{V_2} \quad (16)$$

The mass flows for Equations 15-16 are calculated using Equation 9, where the upstream and downstream pressures are the pressures on either side of the orifice through which the mass is flowing. The upstream pressure is whichever pressure is greater between the two. The model follows the convention where a positive mass flow indicates mass flowing into the control volume. The mass flow is a function of the orifice area and the upstream and downstream pressures. Equation 9 can be summarized as:

$$\dot{m} = A_v \psi(P_u, P_d) \quad (17)$$

The upstream and downstream pressures vary for each control volume, and the flow of air through each orifice as used in Equations 15-16 is described by the following equations:

$$\dot{m}_{exhaust} = \begin{cases} A_{exhaust} \psi(P_{exhaust}, P_1) & \text{if } P_{exhaust} > P_1 \\ -A_{exhaust} \psi(P_1, P_{exhaust}) & \text{if } P_{exhaust} \leq P_1 \end{cases} \quad (18)$$

$$\dot{m}_{leak} = \begin{cases} A_{leak} \psi(P_2, P_1) & \text{if } P_2 > P_1 \\ -A_{leak} \psi(P_1, P_2) & \text{if } P_2 \leq P_1 \end{cases} \quad (19)$$

$$\dot{m}_{vent1} = \begin{cases} A_{vent} \psi(P_{atm}, P_1) & \text{if } P_{atm} > P_1 \text{ and } z > z_{vent} \\ -A_{vent} \psi(P_1, P_{atm}) & \text{if } P_{atm} \leq P_1 \text{ and } z > z_{vent} \\ 0 & \text{otherwise} \end{cases} \quad (20)$$

$$\dot{m}_{vent2} = \begin{cases} A_{vent}\psi(P_{atm}, P_2) & \text{if } P_{atm} > P_2 \text{ and } z < z_{vent} \\ -A_{vent}\psi(P_2, P_{atm}) & \text{if } P_{atm} \leq P_2 \text{ and } z < z_{vent} \\ 0 & \text{otherwise} \end{cases} \quad (21)$$

$$\text{where } z_{vent} = L_1 - \frac{D}{2} \quad (22)$$

$$\dot{m}_{cv} = \begin{cases} A_{cv}\psi(P_{supply}, P_2) & \text{if } P_{supply} > P_2 \\ -A_{cv}\psi(P_2, P_{supply}) & \text{if } P_{supply} \leq P_2 \end{cases} \quad (23)$$

The orifice area used in the mass flow calculations is determined using Equation 13 in all cases except the leakage. The area of the leakage around the ball is given by:

$$A_{leak} = \frac{\pi}{4}(D_{tube}^2 - D_{ball}^2) \quad (24)$$

For the mass flow through the check valve, \dot{m}_{cv} , the area is a function of the check valve dynamics. The maximum orifice area through the check valve is calculated with Equation 13. The check valve is modeled as a mass-spring-damper system, with displacement limiters set to correspond to the check valve's maximum orifice area. The displacement of the mass-spring-damper check valve system while in motion is given by the equation:

$$\ddot{y} = \frac{1}{m_{cv}} [A_{cscv}(P_2 - P_{supply} - P_{crack}) - b_{cv}\dot{y} - k_{cv}y] \quad (25)$$

where y is the displacement of the mass, P_{supply} is the supply pressure downstream from the check valve, P_{crack} is the cracking pressure to open the check valve, A_{cscv} is the cross-sectional area of the check valve mass, and m_{cv} , k_{cv} , and b_{cv} are the mass, spring, damper values that describe the system.

Multiplying the displacement by the circumference of the mass yields the orifice area of the check valve, which is limited by the saturation of the displacement.

$$A_{cv} = 2\pi r_{cv}y \quad (26)$$

The displacement is initiated at $y = 0$, so the orifice area of the check valve is zero until P_2 exceeds the force necessary to move the mass, opens the check valve, and allows air to flow out of V_2 . When P_2 drops, the restorative forces close check valve bringing its mass displacement and orifice area back to zero.

D. Energy

The transfer of energy between the potential pressure energy in the primary control volumes, the ball, and the energy entering and leaving the system through the vent and check valve is also modeled. To accurately compare the total amount of energy in the system, the potential pressure energy is calculated as the total amount of work that the air is capable of doing. This energy is given by:

$$E_{pressure} = \frac{PV}{\gamma - 1} \quad (27)$$

This potential pressure energy is transferred from the exhaust gas to the ball and then back to another control volume of air. The total energy stored in the ball is given by the sum of its kinetic and gravitational potential energy:

$$E_{ball} = KE + PE = \frac{1}{2}m\dot{z}^2 + mgz \quad (28)$$

The total energy reclaimed by the system is calculated using Equation 27 and utilized to compare the dynamic model to the experimental results as well as to calculate the overall system efficiency.

E. Energy Reclamation and Efficiency

The energy reclaimed through the check valve is a function of the pressure increase seen in the tank. Equation 27 is used to calculate the energy. The volume and heat capacity ratio γ are constant, so the energy reclaimed is described by the pressure differential in the tank. The pressure differential is the increase in pressure experienced by a single reclamation event.

$$E_{reclaimed} = \frac{(P_{tank2} - P_{tank1})V_{tank}}{\gamma - 1} \quad (29)$$

The exhaust energy is calculated using the difference between the total potential energy of the exhaust and the energy stored in the same air at atmospheric pressure. Using the assumption of adiabatic expansion, the volume at which the exhaust air has expanded to reach atmospheric pressure is given by:

$$V_f = \left(\frac{P_{exhaust}}{P_{atm}}\right)^{\frac{1}{\gamma}} V_{exhaust} \quad (30)$$

The potential energy in the exhaust volume is the difference between the total energy (given by Equation 27) and the energy datum at P_{atm} and V_f . This difference is given by:

$$E_{exhaust} = \frac{P_{exhaust}V_{exhaust} - P_{atm}V_f}{\gamma - 1} \quad (31)$$

Substituting Equation 30 into Equation 31 results gives the following description of the potential energy in the exhaust gas.

$$E_{exhaust} = \frac{\left[P_{exhaust} - P_{atm} \left(\frac{P_{exhaust}}{P_{atm}}\right)^{\frac{1}{\gamma}} \right] V_{exhaust}}{\gamma - 1} \quad (32)$$

The overall efficiency of the system is calculated by dividing the energy reclaimed by the energy stored as potential pressure energy in the exhaust gas.

$$\eta = \frac{E_{reclaimed}}{E_{exhaust}} \quad (33)$$

These energies are described by Equations 29 and 32. Simplifying gives the efficiency equation:

$$\eta = \frac{(P_{tank2} - P_{tank1})V_{tank}}{\left[P_{exhaust} - P_{atm} \left(\frac{P_{exhaust}}{P_{atm}}\right)^{\frac{1}{\gamma}} \right] V_{exhaust}} \quad (34)$$

Experimental Validation of the Model

A. Experimental Setup

The pneumatic boost converter, shown in Figure 3 - 4, was fabricated using mild steel tube stock with the inner diameter honed and finished to minimize leakage and friction with the ball. The ball is tight-tolerance hardened 440C stainless steel.

An adjuster was fabricated from mild steel for the top of the pneumatic boost converter. It allows the upper control volume to be easily varied for experimental purposes by adjusting L_2 of Figure 3 - 2. A final design need not be adjustable. An oil-resistant Buna-N multipurpose O-ring (dash number 016) is used at the bottom of the adjuster to create a seal. The bottom of the adjuster is threaded with a 1/8 NPT tap to fit a check valve (SMC part no. AKH07B-N01S) that is modified to minimize dead volume. The top of the adjuster is threaded with a 1/8 NPT tap to connect to a sealed tank at constant volume to simulate the supply. The tank (Parker part no. HSSC20-2BD) is a 500 cc stainless steel tank. In practice, the pneumatic boost converter would output directly to the supply line, but the tank is necessary to measure the amount of energy reclaimed through the check valve for the purposes of model validation. A pressure sensor (Festo part no. SPTW-P10R-G14-VD-M12) is used to measure the pressure increase in the tank.

At the bottom of the pneumatic boost converter another, faster pressure sensor (Kulite part no. ETL-375-100A) is used to record the pressure at the device inlet beneath the ball. Data from both pressure sensors is acquired using MATLAB Simulink Real-Time with a Windows target machine. A data acquisition card (National Instruments part no. PCI-6229) is used for valve actuation and pressure sensor data acquisition. Opposite the Kulite pressure sensor, a 2-way valve (Clippard part no. ET-2M-24VDC) allows the lower control volume to vent to atmosphere so the ball can return to its starting position after the reclamation event is complete. At the pneumatic boost converter inlet, a 1/8 NPT thread connects the device to the exhausting cylinder. A 4-way solenoid valve (Bimba part no. M4V230C-08-24VDC) controls the actuation of a 2-way pneumatic cylinder (Bimba part no. 176-DXDEV) and routes the exhaust to the pneumatic boost converter.

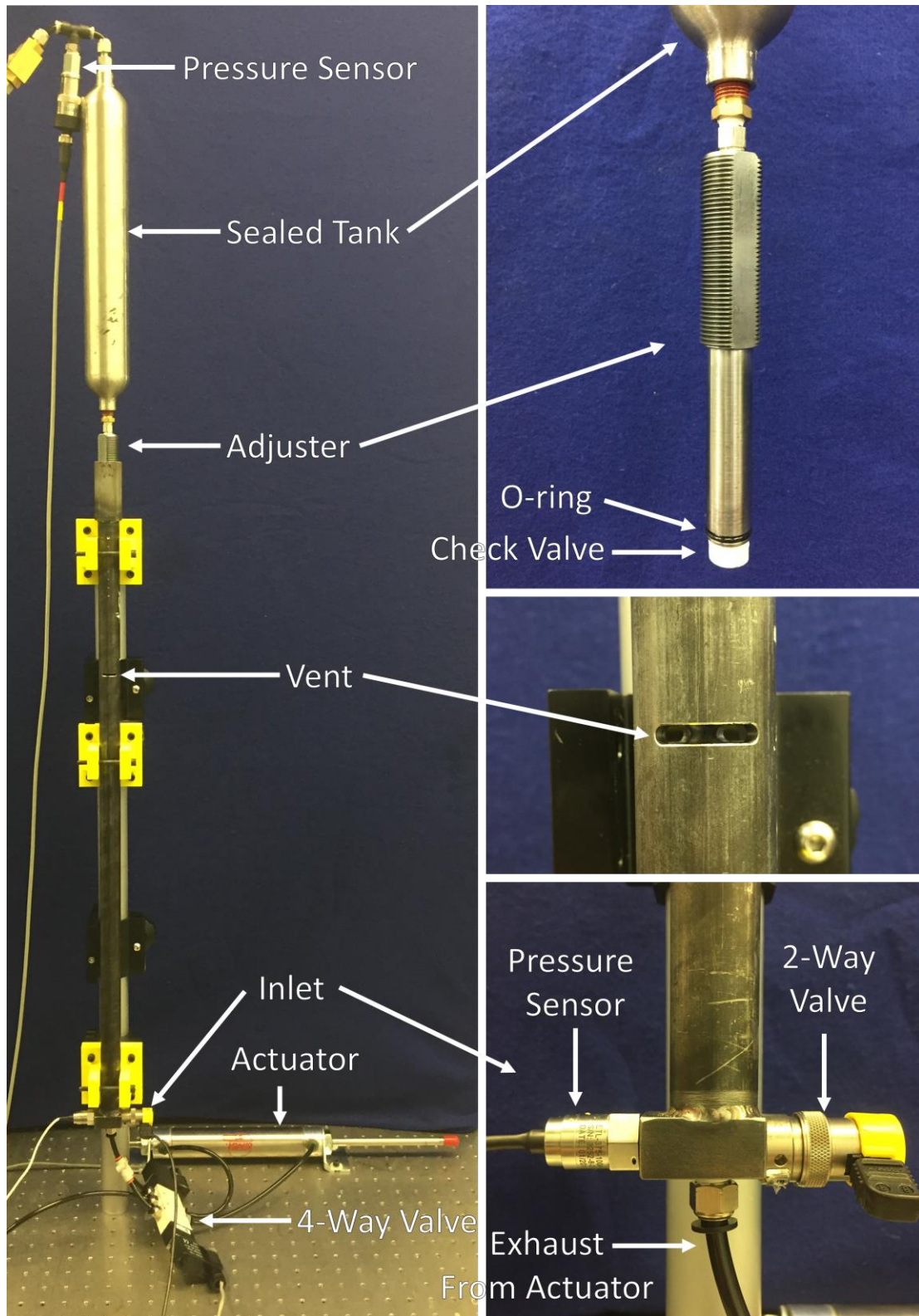


Figure 3 - 4: Annotated photograph of the pneumatic boost converter with close-up views of the adjuster, vent, and system inlet

B. Boost Converter Parameters

The pneumatic boost converter model was validated by conducting experiments and collecting data with the two pressure sensors to compare the simulated and experimental results. Tests were performed with various values for L_2 (by moving the adjuster at the top of the boost converter) and supply pressure. The parameters of the pneumatic boost converter prototype used for these experiments are shown in Table 3 - 2 below.

Table 3 - 2: Pneumatic boost converter model parameters

| | | |
|---|---------------|------------------------|
| Boost converter and ball diameter | D | 19.05 mm |
| Radial gap between ball and tube | R_{gap} | 0.00105 mm |
| Length from bottom to vent | L_1 | 559 mm |
| Length from vent to top | L_2 | 53.3 – 142.2 mm |
| Actuator diameter | D_{piston} | 38.1 mm |
| Actuator length | L_{piston} | 152.4 mm |
| Length of tubing connecting actuator to solenoid | $L_{tubing1}$ | 254 mm |
| Length of tubing connecting solenoid to boost converter inlet | $L_{tubing2}$ | 322.1 mm |
| Tubing inner diameter | D_{tubing} | 4.15 mm |
| Discharge coefficient | C_d | 0.8 |
| Total vent area | A_{vent} | 140.47 mm ² |
| Effective area through solenoid | $A_{exhaust}$ | 11.38 mm ² |
| Effective area through inlet | A_{inlet} | 6.16 mm ² |
| Effective area between ball and tube | A_{leak} | 1.60 mm ² |
| Effective area through check valve | A_{cv} | 6.50 mm ² |
| Radius of check valve | r_{cv} | 1.94 mm |
| Cross-section area of check valve | A_{cscv} | 11.82 mm ² |
| Check valve displaced mass | m_{cv} | 3.39e-8 kg |
| Check valve spring constant | k_{cv} | 56 mN/mm |
| Check valve damping constant | b_{cv} | 2.76e-4 mN-s/mm |
| Check valve cracking pressure | P_{crack} | 5 kPa |
| Room temperature | T_{room} | 293 K |
| Sealed volume beyond the check valve | V_{tank} | 5.19e5 mm ³ |
| Dead volume at bottom below ball | $V_{deadbot}$ | 110 mm ³ |
| Dead volume at top above ball | $V_{deadtop}$ | 1220 mm ³ |

Parameters were either measured directly (as with dead volumes), approximated using given manufacturer data (as with effective orifice areas via flow coefficients or tolerances), or approximated experimentally (as with check valve mass and spring values).

C. Effective Damping

The parameters for the dynamic model were either measured or calculated from manufacturer data. The only remaining parameter necessary for the dynamic model was the effective coefficient of damping of Equation 1. This damping coefficient, b , allows for the calculation of a damping force that encompasses all of the resistive, velocity-dependent forces acting on the ball in the pneumatic boost converter.

$$F_d = -b\dot{z} \quad (35)$$

The primary source of damping is the viscous damping between the ball and tube with a mixture of air and lubricant between them.

With all other model parameters known, the value for the coefficient of damping was tuned to match the experimental data. The effective damping coefficient was tuned such that the pressures measured at the exhaust and past the reclaiming check valve were reasonably consistent with the expected pressures determined by the dynamic model. The damping coefficient was chosen to be $0.26 \frac{N \cdot s}{m}$ in order to accurately model the damping forces in the pneumatic boost converter.

D. Experimental vs. Simulated Pressures

To validate the model, experimental data was taken at different pressures and different values for L_2 , which was modified by moving the upper adjuster. The system was designed to operate with a supply of 653 kPa (80 psig), but additional information describing the system's behavior at 584 kPa (70 psig) is useful in validating the model's description of the system.

The relevant pressures to be compared are the exhaust pressure and the pressure in the tank past the check valve. The exhaust pressure is the pressure below the ball at the pneumatic boost converter inlet. It measures the pressure of the volume of air below the ball, including the volume in the pneumatic boost converter, the tubing connecting to the exhaust, and the exhausting cylinder itself. This pressure oscillates as the ball bounces across the vent, where it eventually settles. The tank pressure measures the pressure in the sealed, constant volume of air beyond the check valve. The pressure change in this volume is used to calculate the mass and energy of the air being reclaimed through the check valve. This pressure sensor records large oscillations before settling to a reasonable pressure. These are not true pressure fluctuations, but rather a result of the pressure dynamics occurring faster than the sensor can accurately measure. These results demonstrate an accurate model of the pneumatic boost converter that consistently predicts both measured pressures. Numerous trials were run for each set of conditions; Figures 3 - 5 to 3 - 10 show typical results for three experimental sets.

Each experimental set begins with the tank filled at the supply pressure. The cylinder is consecutively actuated six times, with adequate time between trials to reset the system. Between actuations the ball returns to its starting position, but the tank pressure is not reset. So a small increase in tank pressure is experienced between the six actuations of a single experimental set. The dynamic model indicates that the tank is large enough to result in pressure increases small enough to have no significant impact on the results of subsequent tests.

The following figures show a single reclamation event occurring when the cylinder actuates. This event is one of six consecutive trials per set. Each of the six actuations is very similar (see Figure 3 - 11), and the chosen events are representative of the experimental set. Each trial is described by two figures. The first figure in each pair shows the exhaust pressure below the ball. The second figure in each pair shows the tank pressure as energy is reclaimed through the check valve.

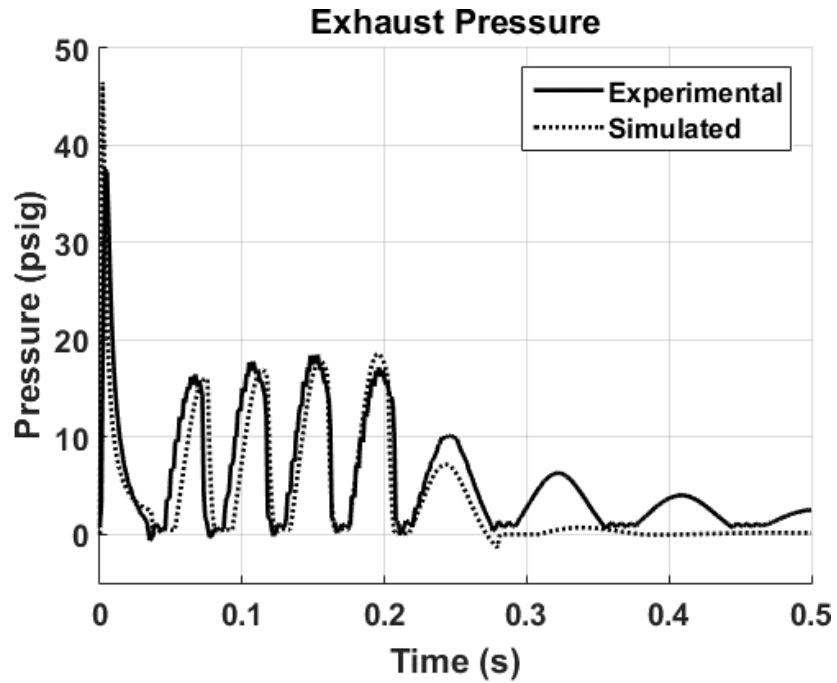


Figure 3 - 5: Experimental and simulated exhaust pressures with roughly 653 kPa (80 psig) supply pressure and an L_2 of 91.4 mm

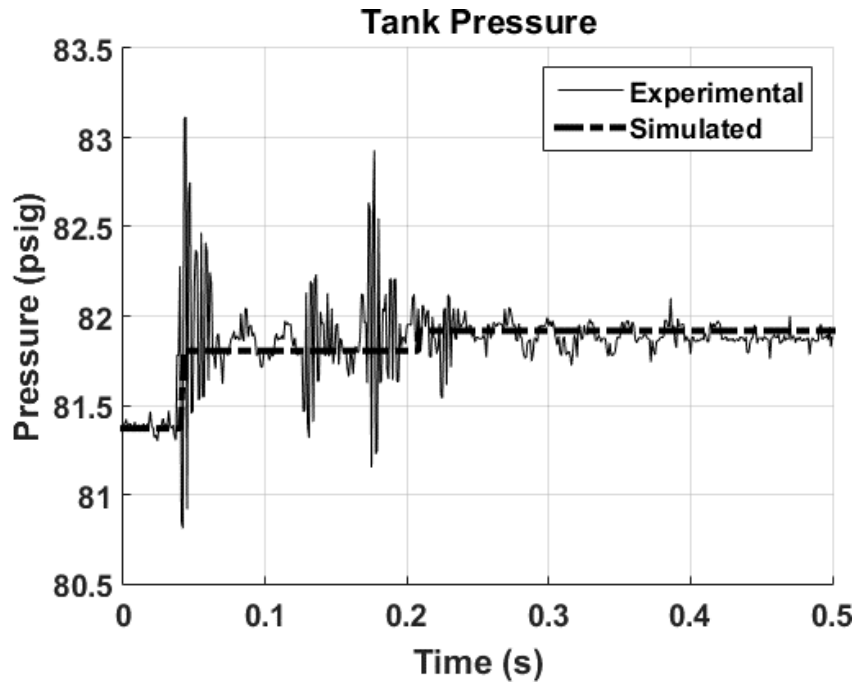


Figure 3 - 6: Experimental and simulated tank pressures with roughly 653 kPa (80 psig) supply pressure and an L_2 of 91.4mm

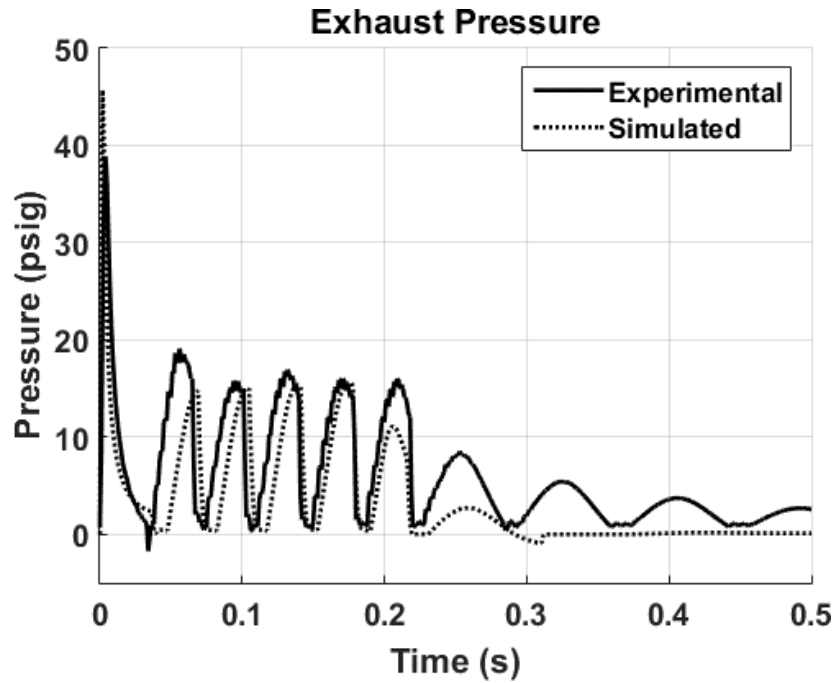


Figure 3 - 7: Experimental and simulated exhaust pressures with roughly 653 kPa (80 psig) supply pressure and an L_2 of 53.3 mm

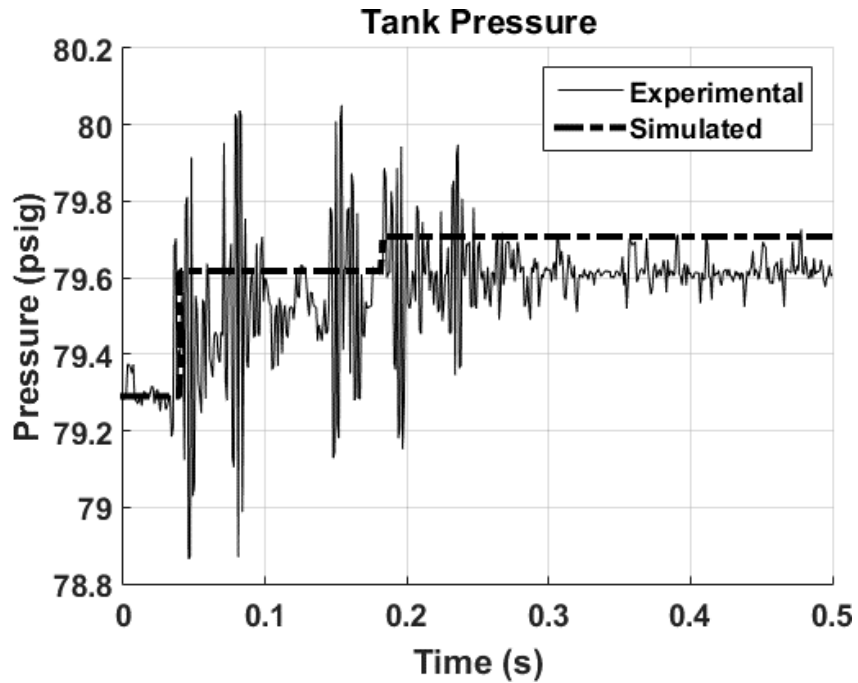


Figure 3 - 8: Experimental and simulated tank pressures with roughly 653 kPa (80 psig) supply pressure and an L_2 of 53.3 mm

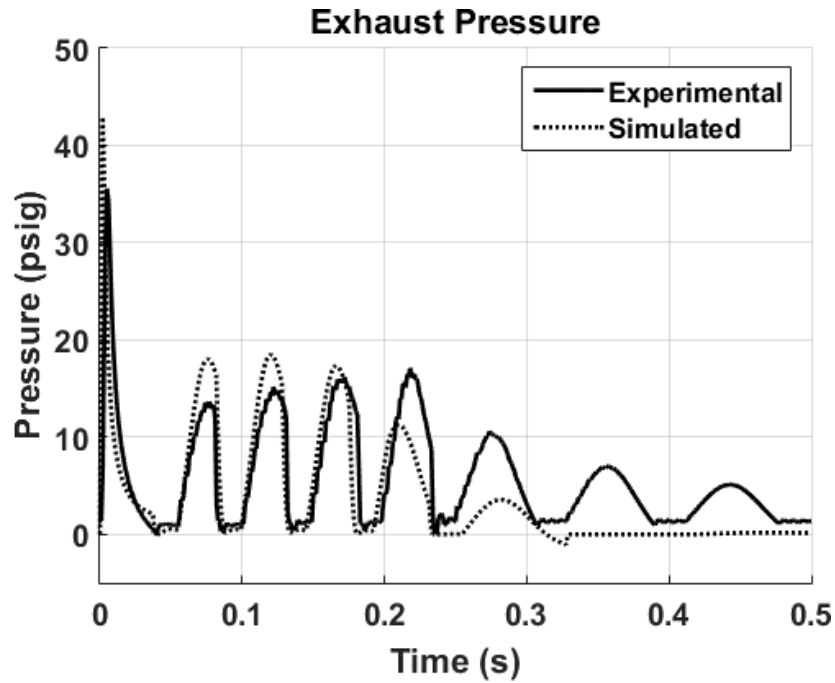


Figure 3 - 9: Experimental and simulated exhaust pressures with roughly 584 kPa (70 psig) supply pressure and an L_2 of 116.8 mm

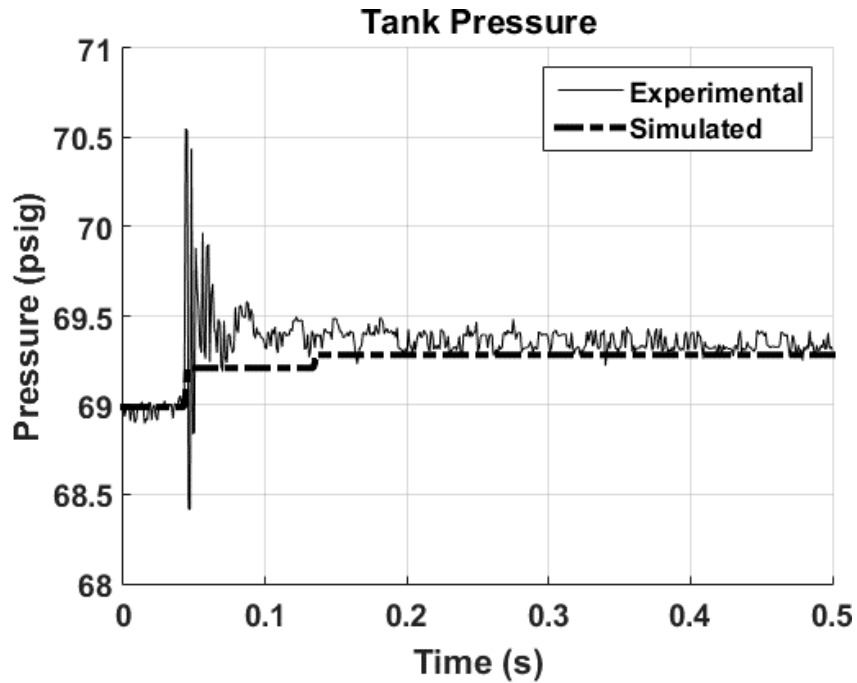


Figure 3 - 10: Experimental and simulated tank pressures with roughly 584 kPa (70 psig) supply pressure and an L_2 of 116.8 mm

The dynamics of the system are fairly consistent between trials, but small inconsistencies like the amount of sliding versus rolling done by the ball make it impossible for the dynamic model to perfectly

predict the experimental results. The exhaust and tank pressures for six consecutive trials are overlaid in the figures below to illustrate the system's consistency.

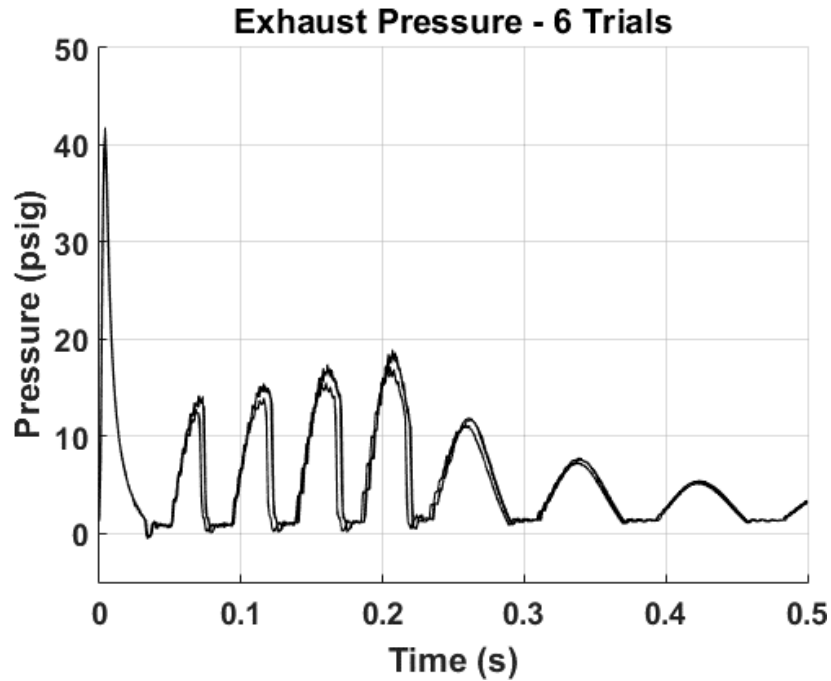


Figure 3 - 11: Experimental exhaust pressures from six consecutive actuations overlaid

The initial pressure in the tank varies with each actuation, so an overlay of consecutive actuations does not directly coincide. However it does demonstrate the consistent nature of the pneumatic boost converter.

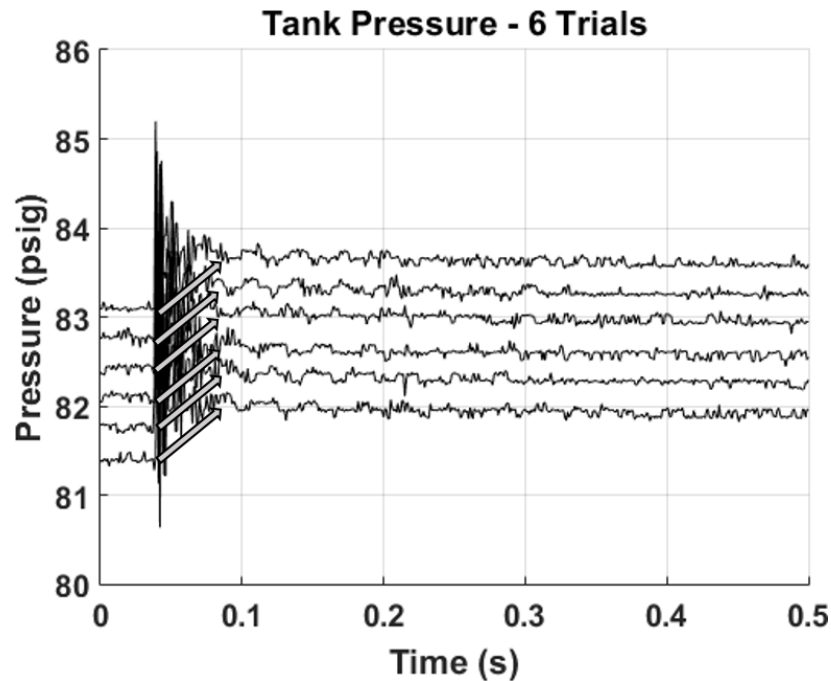


Figure 3 - 12: Experimental tank pressures from six consecutive actuations overlaid

The results of the experiments shown above and more are summarized in Figure 3 - 13 and Table 3 - 3 below. The pressure increase in the tank predicted by the dynamic model and achieved by the experiments are compared. There are two experiments at 91.4 mm where the upper volume adjuster was replaced with a longer variant to accommodate additional experiments, increasing the range of L_2 . The matching results of these tests confirm that there was no difference between the two adjusters. The figure below shows the experimental and simulated pressure increases, and the error bars indicate the entire range of pressure increases seen by the six experimental actuations for each configuration.

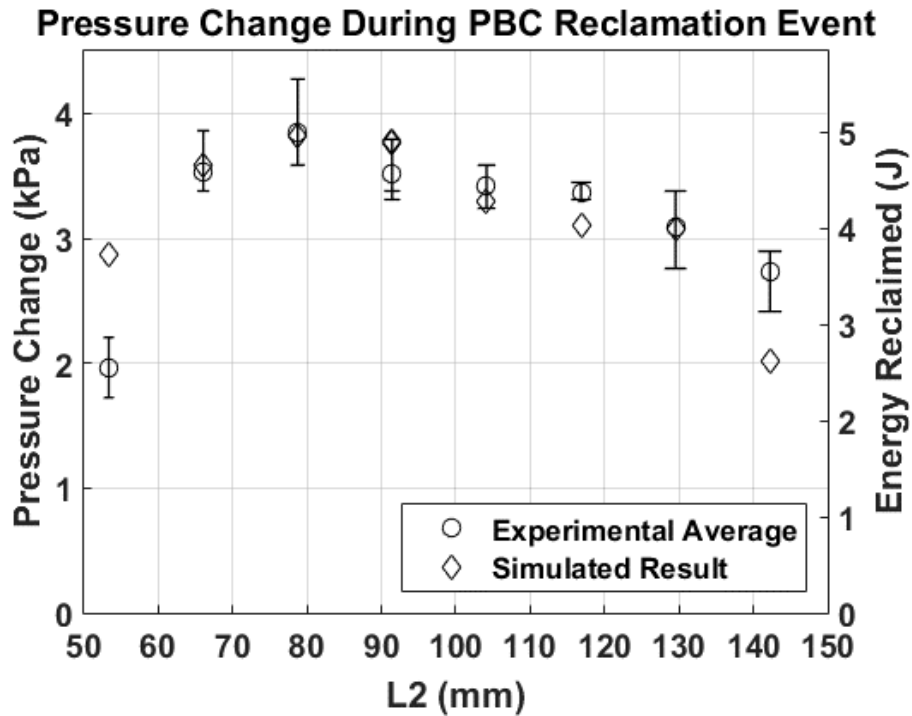


Figure 3 - 13: Experimental and simulated results at 653 kPa (80 psig) supply

Excluding the endpoints, the simulated pressure changes fall within the range of experimental values for all cases but one. In the case where L_2 is 116.8 mm, the simulated result is outside the range of experimental values, but this is due to the uncommon precision of that experimental set. The final experiments with L_2 at 53.3 mm resulted in the failure of the check valve due to collisions with the steel ball. This would account for the significantly reduced pressure increase at the lower end of the L_2 range.

The results shown in Table 3 - 3 utilize the simulated and average experimental pressure increases in the tank in order to identify the total energy reclamation per actuation event (given by Equation 29) and the total system efficiency (given by Equation 34). The percent error is the difference between the simulated results and the average experimental results.

Table 3 - 3: Comparison of simulated and experimental tank pressure changes

| Supply Pressure | L_2 | Pressure Increase (kPa) | Energy Reclaimed (J) | System Efficiency (%) | Mean Percent Error |
|-------------------|----------|--------------------------|--------------------------|--------------------------|--------------------|
| 653 kPa (80 psig) | 142.2 mm | Sim: 2.015 Exp: 2.735 | Sim: 2.615 Exp: 3.549 | Sim: 2.221 Exp: 3.015 | 35.75 |
| 653 kPa (80 psig) | 129.5 mm | Sim: 3.082 Exp: 3.091 | Sim: 4.000 Exp: 4.011 | Sim: 3.395 Exp: 3.405 | 0.29 |
| 653 kPa (80 psig) | 116.8 mm | Sim: 3.104 Exp: 3.367 | Sim: 4.028 Exp: 4.370 | Sim: 3.444 Exp: 3.736 | 8.47 |
| 653 kPa (80 psig) | 104.1 mm | Sim: 3.292 Exp: 3.424 | Sim: 4.272 Exp: 4.444 | Sim: 3.614 Exp: 3.758 | 4.01 |
| 653 kPa (80 psig) | 91.4 mm | Sim: 3.761 Exp: 3.516 | Sim: 4.881 Exp: 4.563 | Sim: 4.016 Exp: 3.755 | -6.51 |
| 653 kPa (80 psig) | 91.4 mm | Sim: 3.776 Exp: 3.516 | Sim: 4.900 Exp: 4.563 | Sim: 4.023 Exp: 3.746 | -6.89 |
| 653 kPa (80 psig) | 78.7 mm | Sim: 3.825 Exp: 3.850 | Sim: 4.964 Exp: 4.997 | Sim: 4.094 Exp: 4.120 | 0.65 |
| 653 kPa (80 psig) | 66.0 mm | Sim: 3.581 Exp: 3.528 | Sim: 4.647 Exp: 4.579 | Sim: 3.833 Exp: 3.776 | -1.48 |
| 653 kPa (80 psig) | 53.3 mm | Sim: 2.863 Exp: 1.965 | Sim: 3.716 Exp: 2.550 | Sim: 3.145 Exp: 2.159 | -31.37 |
| 584 kPa (70 psig) | 116.8 mm | Sim: 1.999 Exp: 2.537 | Sim: 2.595 Exp: 3.293 | Sim: 2.592 Exp: 3.290 | 26.90 |
| 584 kPa (70 psig) | 104.3 mm | Sim: 2.344 Exp: 2.806 | Sim: 3.042 Exp: 3.642 | Sim: 3.023 Exp: 3.618 | 19.71 |
| 584 kPa (70 psig) | 91.6 mm | Sim: 3.241 Exp: 3.158 | Sim: 4.206 Exp: 4.098 | Sim: 4.161 Exp: 4.055 | 2.55 |

Conclusion

The pneumatic boost converter and a dynamic model that accurately describes it have been presented and validated with experimental data. The model describes the dynamics of the system including the movement of the ball, the changing pressures and volumes within the system, and the mass exchange between volumes. The parameters used by the dynamic model were entirely known, with the exception of the effective damping coefficient within the system. Tuning the damping coefficient to a reasonable value in order to match the behavior of the system gave a simulation of the pneumatic boost converter using only one tunable parameter. The data shows that the simulation is capable of predicting the results of the pneumatic boost converter fairly accurately. The simulation performs noticeably better for tests conducted within the recommended operating range for which it was designed, but loses accuracy at the prototype

limits. The average percent error for the total energy reclaimed across all trials is 12.05%. The average percent error within the recommended operating range (653 kPa & 66 to 130 mm) is 4.04%. The results of the simulated and experimental tests both indicate that there is a value for L_2 that would maximize the performance of the system. Initially, reducing L_2 decreases the volume of air that needs to be compressed and reclaimed. However, at a certain point further reductions inhibit the system and decrease its efficiency. The largest contributor to this decrease in performance is the energy loss due to the collision of the ball with the check valve.

The first prototype for the pneumatic boost converter was able to successfully reclaim some energy from the exhaust gas discharge of a pneumatic cylinder. The dynamic model effectively validates the performance of the system and is valuable in determining the source of losses within the system. The model suggests that removing the effects of viscous damping would nearly double the amount of energy reclaimed per actuation. While the system efficiency of this pneumatic boost converter laboratory prototype is too low to reclaim a significant portion of the wasted exhaust energy, it provides evidence that the link between the electrical and pneumatic boost converters is realizable. The dynamic model and prototype validate the energetic equivalence drawn to the electrical boost converter that inspired this device. It is possible that the inertia of the boost converter could be recognized in another, more efficient form, perhaps as a cylindrical mass or as an expandable bladder. Understanding the relationship between the individual components in both energetic domains encourages the future design of additional pneumatic systems utilizing existing electrical converters.

Acknowledgment

This work was supported by a grant from the National Fluid Power Association.

References

- [1] Love, L.J., Lanke, E., and Alles, P., 2012, "Estimating the Impact (Energy, Emissions and Economics) of the U.S. Fluid Power Industry," Oak Ridge National Laboratory, Oak Ridge, TN.
- [2] Price, L. and Hasanbeigi, A., 2010, "Industrial Energy Audit Guidebook: Guidelines for Conducting an Energy Audit in Industrial Facilities," Ernest Orlando Lawrence Berkeley National Laboratory, Berkeley, CA.
- [3] Cramer, D. N. and Barth, E.J., "Pneumatic Strain Energy Accumulators for Exhaust Gas Recycling," *Proceedings of the ASME/Bath 2013 Symposium on Fluid Power and Motion Control*, FPMC2013-4488, October 6-9, 2013, Sarasota, Florida USA.
- [4] Pedchenko, A. and Barth, E.J., "Design and Validation of a High Energy Density Elastic Accumulator Using Polyurethane," *Proceedings of the ASME 2009 Dynamic Systems and Control Conference*, pp. 283-290, October 12-14, 2009, Hollywood, California USA.

- [5] Cummins, J.J., Pedchenko, A., Barth, E.J., and Adams, D.E., "Advanced Strain Energy Accumulator: Materials, Modeling and Manufacturing." *Proceedings of the ASME/Bath 2014 Symposium on Fluid Power and Motion Control*, FPMC2014-7840, September 10-12, 2014, Bath, England UK.
- [6] Cummins, J.J., Thomas, S., Nash, C., Mahadevan, S., Barth, E.J., and Adams, D.E., "Experimental Evaluation of the Efficiency of a Pneumatic Strain Energy Accumulator," *International Journal of Fluid Power*, In Review.
- [7] Cummins, J.J., Barth, E.J., and Adams, D.E., "Modeling of a Pneumatic Strain Energy Accumulator for Variable System Configurations With Quantified Projections of Energy Efficiency Increases," *Proceedings of the ASME/Bath 2015 Symposium on Fluid Power and Motion Control*, FPMC2015-9605, October 12-14, 2015, Chicago, Illinois USA.
- [8] Eichhorn, T., 2008, "Boost Converter Efficiency Through Accurate Calculations." Power Electronics Technology, Grass Valley, CA.
- [9] Mohan, N., Undeland, T.M., and Robbins, W.P., 2003, *Power Electronics*, John Wiley & Sons, Inc., New Jersey.
- [10] Gibson, T. and Barth, E.J., "Dynamic Equivalence of Pneumatic and Electrical Boost Converters for Exhaust Gas Energy Reclamation," *Proceedings of the ASME/Bath 2016 Symposium on Fluid Power and Motion Control*, FPMC2016-1786, September 7-9, 2016, Bath, England UK.
- [11] Richer, E., and Hurmuzlu, Y., 2000, "A High Performance Pneumatic Force Actuator System: Part I—Nonlinear Mathematical Model." *ASME Journal of Dynamic Systems, Measurement, and Control* 122, pp. 416-425.

CHAPTER IV. FUTURE DIRECTIONS

This thesis has presented the work of two manuscripts that detail the design of a pneumatic boost converter proposed to recycle the wasted exhaust gas energy of pneumatic systems. The inspiration for this device was drawn from electrical boost converters. An energetic equivalence between the electrical and pneumatic domains allows for the design to be translated to a pneumatic device using energetically analogous components. A first principles dynamic model was developed to describe the device, and the model was used to develop a prototype by simulating the response of the system. With the prototype, experiments were conducted for comparison to the simulated results of the model. These comparisons were used to tune unmeasurable parameters and validate the model. After tuning, the dynamic model reasonably predicts the behavior of the pneumatic boost converter prototype.

In the experimental results, the pneumatic boost converter was found to reclaim only a small portion of the exhaust gas energy. This is largely a result of losses in the system due to damping, including friction and viscous damping. In future work, the validated dynamic model can be used to further pinpoint the source of inefficiency within the pneumatic boost converter. With this information, it may be possible to modify the device to minimize these inefficiencies and create a device that more effectively reclaims the exhaust gas energy. Alternatively, a different device that utilizes the known energetically equivalent components could be developed that minimizes the viscous friction. For example, replacing the momentum of the ball with an inertia that suffers less from friction and viscous damping would provide a substantial boost to system efficiency.

This work has also validated the energetic analogy between the electrical and pneumatic components used in the boost converters. The boost converter served as the simplest starting point to develop this foundational understanding of the electrical to pneumatic analogy. This information could be utilized in future works to develop new devices based on different electrical converters. There are many electrical converters that are commonly used and well understood that could serve as the basis for an equivalent pneumatic converter. For example, the Ćuk converter is an inverting DC/DC boost converter, which means that it delivers a negative voltage to the load. In the pneumatic domain, this would equate to drawing a vacuum while simultaneously boosting the pressure. The development of such devices would be very beneficial to the pneumatic industry.

APPENDIX A: SIMULINK DIAGRAMS

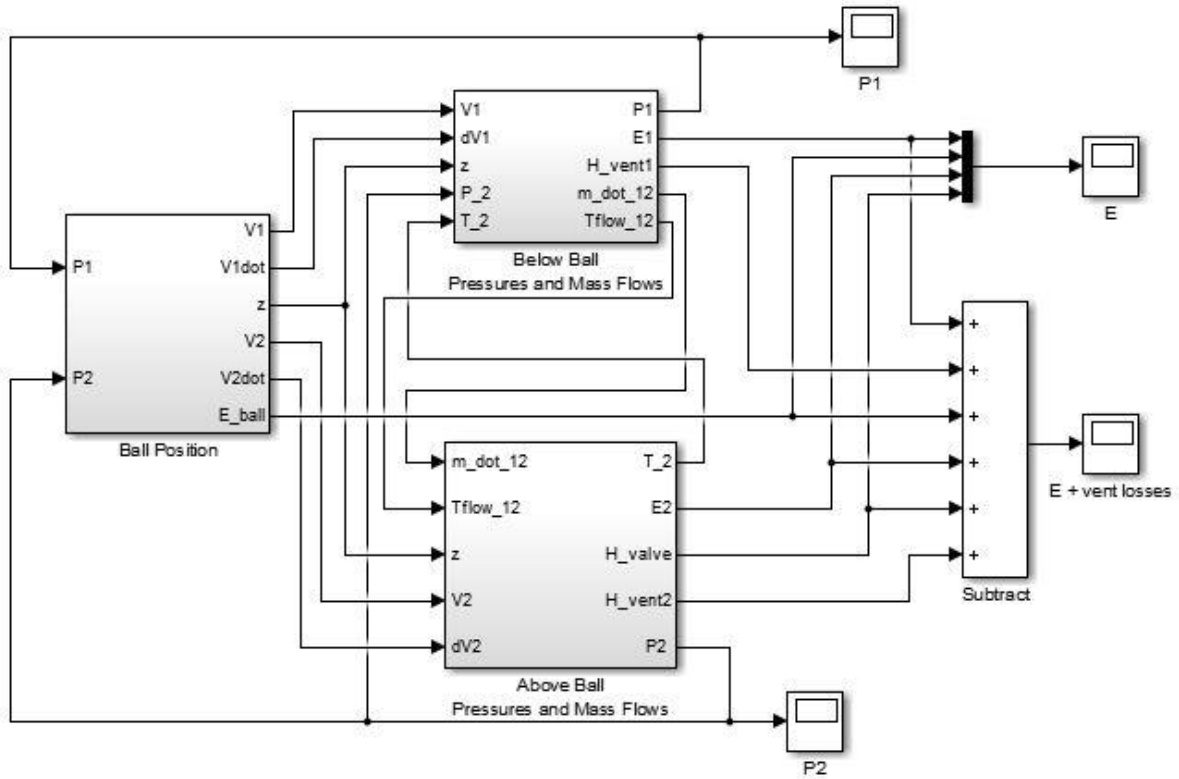


Figure A - 1: Simulink model overview

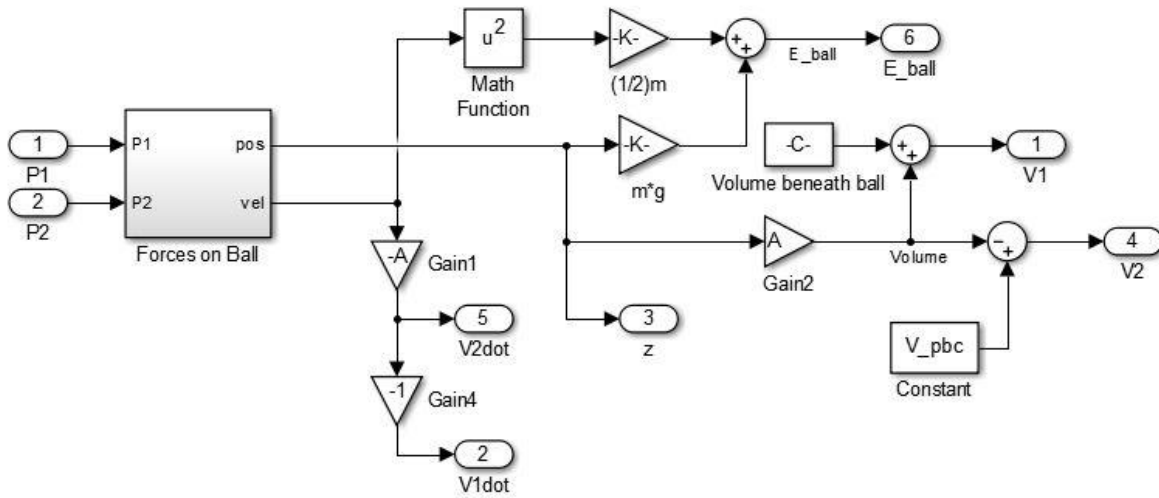


Figure A - 2: Volume calculations and energy of ball

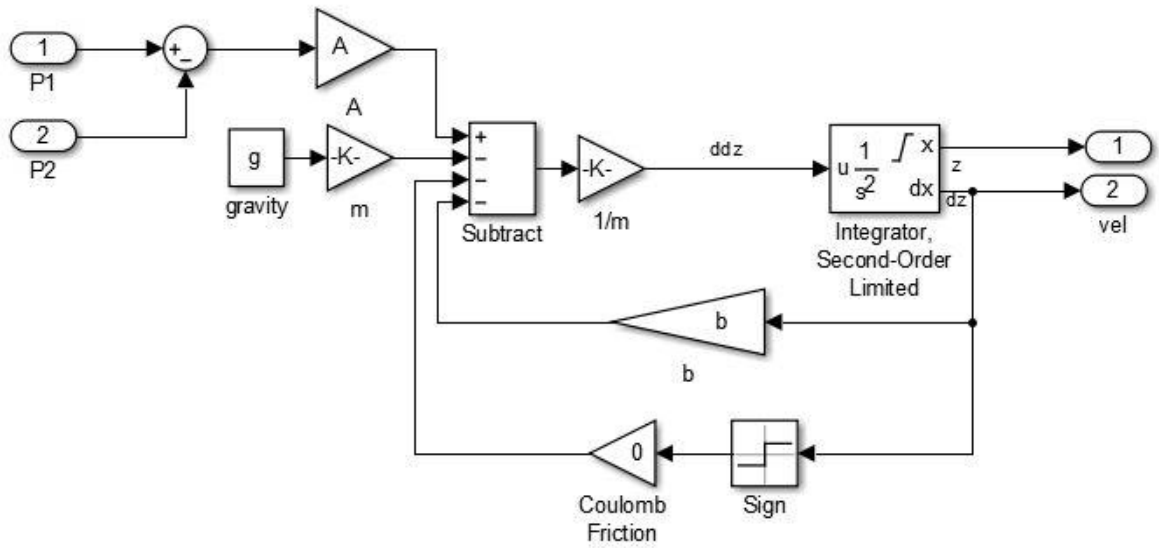


Figure A - 3: Force balance on ball and acceleration integration

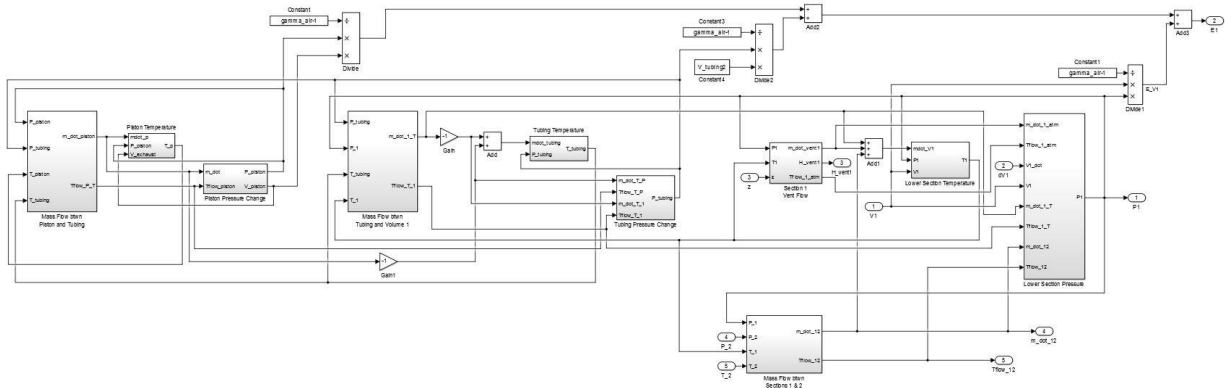


Figure A - 4: Overview of dynamics occurring below the ball including the exhausting cylinder, the connecting tubing, and the pneumatic boost converter

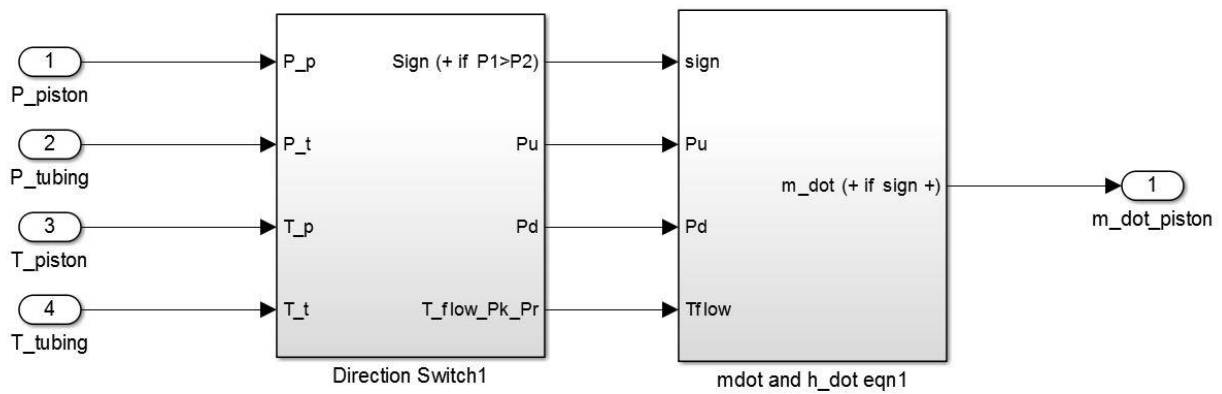


Figure A - 5: Basic mass flow model overview

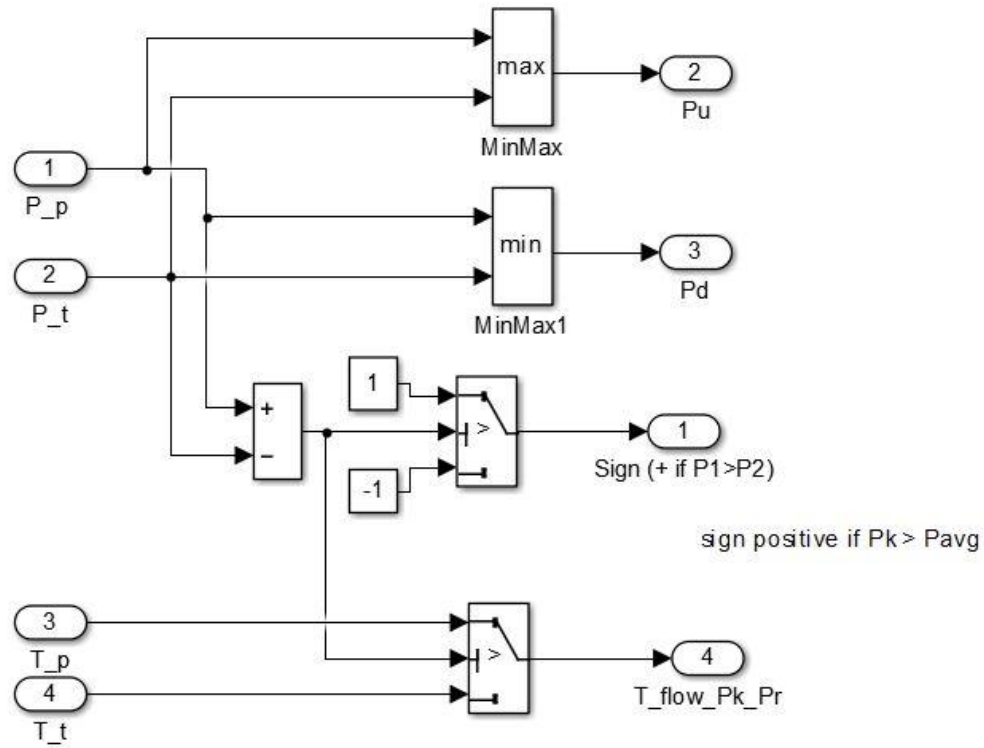


Figure A - 6: Mass flow direction switch

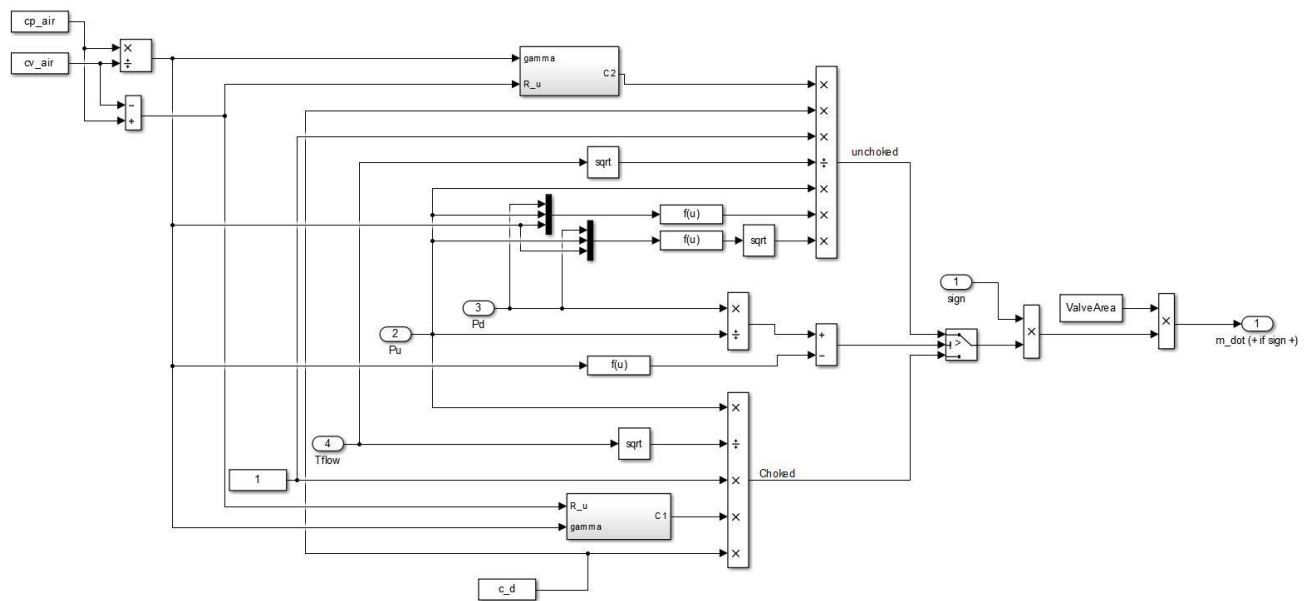


Figure A - 7: Calculation of mass flow through an orifice

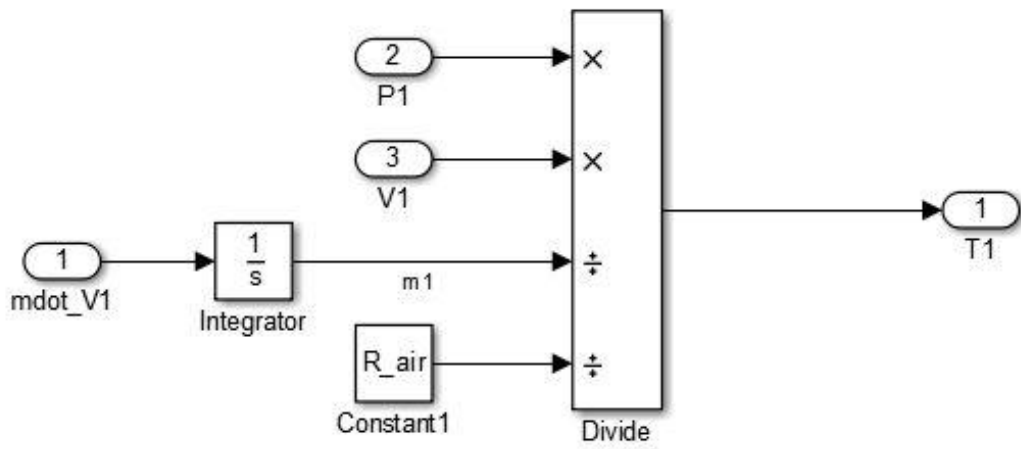


Figure A - 8: Ideal gas law calculation of temperature

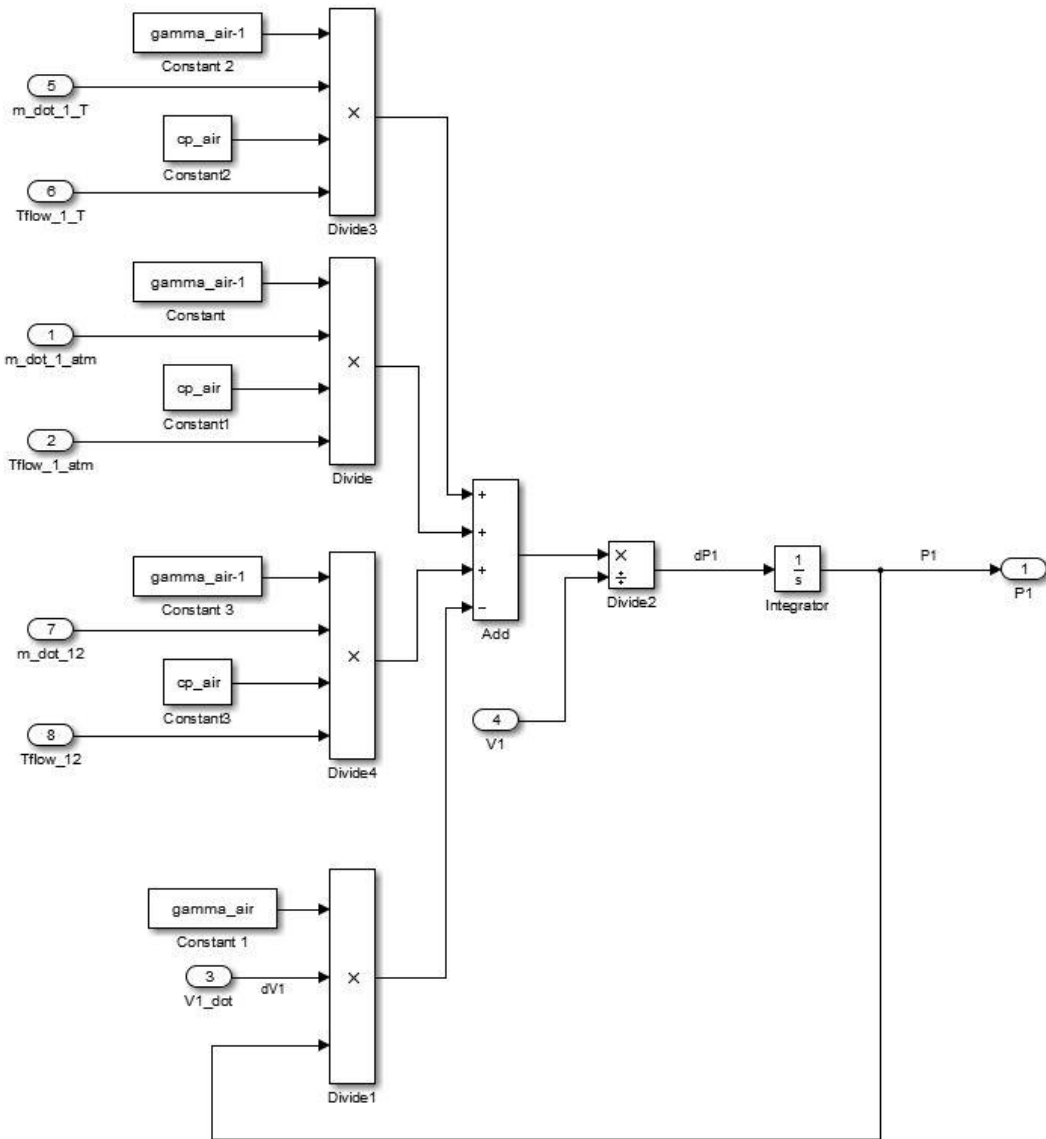


Figure A - 9: Sample calculation for the rate of pressure change given multiple mass flows and integrated to obtain pressure in a volume

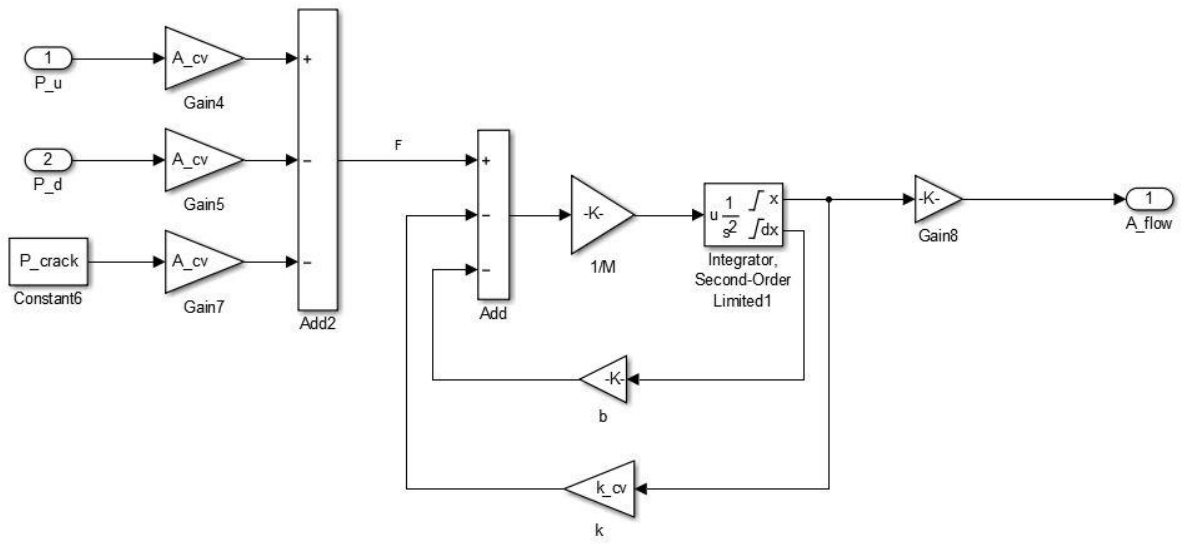


Figure A - 10: Check valve dynamics at the device outlet

APPENDIX B: MATLAB CODE

Dynamic Model Parameters

```
%close all; clear; clc;

% Base Units
% kg, kPa, mm, mN, uJ, uW, s, K

% Test Params
D_piston = 38.1;           % mm (1.5") - Diameter of exhausting piston
L_piston = 152.4;         % mm (6") - Length of exhausting piston

% Constants
P_atm = 101.325;          % kPa - Atmospheric pressure
g = 9806.65;              % mm/s^2 - Gravity
rho = 7.9/1000/1000;      % kg/mm^3 - Density of steel
rho_air = 1.225e-9;       % kg/mm3 - Density of air
visc = 14.8;              % mm2/s - Kinematic viscosity of air
R_air = 287e6;            % uJ/kg/K - Gas constant of air
cp_air = 1012e6;          % uJ/kg/K - Constant pressure specific heat
cv_air = 723.7e6;         % uJ/kg/K - Constant volume specific heat
c_d = 0.8;                % Non-dimensional discharge coefficient
gamma_air = 1.4;         % Heat capacity ratio of air
T_room = 293;            % K (68F) - Room temp
T_exhaust = T_room;      % Temperature of exhaust gas
b = 0.26;                % Effective coefficient of damping (N-s/m)

% Boost Converter Parameters
D = 19.05;                % mm (0.75") - Tube diameter
L1 = 559;                 % mm (22") - Bottom of tube to vent
P_exhaust = P_supply;     % kPa - Pressure of exhaust gas

s_vent_slot = (D/2)*(82.82*pi/180); % mm - Single vent slot arc length
h_vent_slot = 3.175;      % mm (1/8") - Height of vent slot
A_vent = 140.467;         % mm^2 - Area of vent (from
Solidworks)

% System Values
L_total = L1+L2+h_vent_slot; % mm - Total tube length
A = (pi/4)*D^2;           % mm^2 - Tube cross-sectional area
V1 = A*L1;                % mm^3 - Tube volume below vent
V2 = A*L2;                % mm^3 - Tube volume above vent
V_ball = (4/3)*pi*(D/2)^3; % mm^3 - Volume of ball
V_bb = (1/3)*pi*(D/2)^3; % mm^3 - Volume of air trapped
below ball
V_piston = (pi/4)*D_piston^2*L_piston; % mm^3 - Volume of exhaust being
discharged from piston

L_tubing1 = 254;          % mm - length of tubing connecting piston
to valve
L_tubing2 = 322;         % mm - length of tubing connecting valve to
PBC V1
R_tubing = 2.075;        % mm - inner radius of tubing
```

```

A_tubing = pi*R_tubing^2;           % mm^2 - cross-sectional area of tubing
V_tubing1 = A_tubing*L_tubing1;     % mm^3 - volume of tubing connecting
piston to valve
V_tubing2 = A_tubing*L_tubing2;     % mm^3 - volume of tubing connecting
valve to PBC V1

V_dead_bot = 106.88;                % mm^3 - dead
volume btwn PBC inlet and ball
V_dead_top = 1056*1.16;             % mm^3 (700) -
dead volume btwn ball and O-ring
V_pbc = A*L_total + V_dead_top - V_ball - V_bb; % mm^3 - PBC volume
above ball before discharge
V_exhaust = V_piston + V_tubing1;   % mm^3 - Volume in
exhaust at time of discharge
V_tank = 500000 + (pi/4)*10.16^2*152.4 + A_tubing*500; % mm^3 - Volume of
tank (+adjuster +tubing to valve)
m_ball = rho*(pi/6)*D^3;            % kg - mass of ball
m_air_V2 = P_atm*(V2+V_dead_top)/R_air/T_room; % kg - mass of air
above vent
m_air_pbc = P_atm*V_pbc/R_air/T_room; % kg - mass of air
above ball before discharge
m_air_exhaust = P_exhaust*V_exhaust/R_air/T_exhaust; % kg - mass of air
stored in piston before discharge
m_air_tubing = P_atm*V_tubing2/R_air/T_room; % kg - mass of air
stored in tubing between valve and CV0 before discharge
m_air_dead_bot = P_atm*(V_dead_bot+V_bb)/R_air/T_room; % kg - mass of air
stored between inlet and ball before discharge
m_air_dead_top = P_atm*V_dead_top/R_air/T_room; % kg - mass of air
stored between ball and o-ring at max height
m_tank_init = P_tank_init*V_tank/R_air/T_room; % kg - mass of air
in tank before first acutation

% Check Valve Dynamics (SMC:AKH07A-N01S)
r_cv = 1.94;                         % mm - Radius of check
valve
A_cv = pi*r_cv^2;                     % mm^2 - Area of check
valve
P_crack = 5;                          % kPa (0.73 psi) - CV
cracking pressure
R_cv_disk1 = 3;                       % mm - Radius of disk
inside cv
t_cv_disk1 = 1;                       % mm - Thickness of
disk inside cv
rho_cv_disk1 = 1.2e-9;                 % kg/mm^3 - density of
disk (hard rubber)
m_cv = pi*R_cv_disk1^2*t_cv_disk1*rho_cv_disk1; % kg - mass of disk
k_cv = 56;                             % mN/mm - stiffness of
spring in cv
b_cv_eff = 2*0.1*sqrt(k_cv/m_cv)*m_cv; % mN-s/mm - damping in
check valve
x_cv_max = 6.5/pi/2/r_cv;              % mm - max displacement
of cv disk

% Valve Areas
A_sol = 11.383;                       % mm^2 - area of Bimba solenoid orifice

```

```

A_valve = 7 *0.88; % mm^2 - area of Bimba valve
orifice
A_leak = 1.6 *0.99; % mm^2 - area for leakage around
ball

```

PSI to kPa Function

```

% Converts a pressure from gauge PSI to absolute kPa

```

```

function kpa = psikpa(psi)
    kpa = (psi+14.7)*6.89475729;
end

```

kPa to PSI Function

```

% Converts a pressure from absolute kPa to gauge PSI

```

```

function psi = kpaPSI(kpa)
    psi = kpa/6.89475729-14.7;
end

```

Figure Creation Script

```

close all; clear all; clc;

```

```

%% 80 psi, 91 mm
% Loads experimental data, runs parameter script, runs simulation, plots
% experimental and simulated pressures for tank and exhaust
load('C:\Users\gibsontj\Documents\MATLAB\Boost Converter\PBC Workspace Data -
Full L2 Range\04_May_2017_15_29_12.mat')
run('tube_system_params_May22_2017.m');
sim('tube_system_adiabatic_expansion_Mar7_2017_smcCV')
sim_exp_plots(1,t,P_exh,P1,P_tank,TankPressure,L2);

```

```

%% 80 psi, 53 mm
% Loads experimental data, runs parameter script, runs simulation, plots
% experimental and simulated pressures for tank and exhaust
load('C:\Users\gibsontj\Documents\MATLAB\Boost Converter\PBC Workspace Data -
Full L2 Range\04_May_2017_16_01_51.mat')
run('tube_system_params_May22_2017.m');
sim('tube_system_adiabatic_expansion_Mar7_2017_smcCV')
sim_exp_plots(1,t,P_exh,P1,P_tank,TankPressure,L2);

```

```

%% 70 psi, 116 mm
% Loads experimental data, runs parameter script, runs simulation, plots
% experimental and simulated pressures for tank and exhaust
load('C:\Users\gibsontj\Documents\MATLAB\Boost Converter\PBC Workspace Data -
Broken SMC CV (Paper)\02_Mar_2017_19_40_08.mat')
run('tube_system_params_Mar3_2017_smc.m');

```



```

sim('tube_system_adiabatic_expansion_Mar3_2017_smcCV')
sim_exp_plots(1,t,P_exh,P1,P_tank,TankPressure,L2);

%% Overlay 6 actuations from 02_Mar_2017_17_48_56 (80 psi, 116 mm)
run('overlay6trials.m');

%% Error bar plot showing range of experimental values and simulated results
run('errorbar_plot.m');

```

Plot Simulated and Experimental Results

```

function sim_exp_plots(n,t,P_exh,P1,P_tank,TankPressure,L2)
% n selects actuation (1=20s, 2=40s, 3=60s, etc.)

time = t((n*20000+1019):(n*20000+1519)) - (n*20+1.018);
%% Exhaust
figure, grid on, hold on
plot(time,P_exh((n*20000+1019):(n*20000+1519))-14.7,'k','linewidth',2)
plot(P1.time,P1.data*0.145038-14.7,':k','linewidth',2)
xlabel('Time (s)'), ylabel('Pressure (psi)'), title('Exhaust Pressure')
legend('Experimental','Simulated')
set(gca,'FontSize',14,'fontWeight','bold')
set(gcf,'name',['Exhaust Pressure (' num2str(round(P_tank(1))) ' psi & L2 = '
num2str(round(L2,1)) 'mm) '])
yl = ylim(gca); yl(1)=-5; ylim(gca,yl);

%% Tank
figure, grid on, hold on
plot(time,P_tank((n*20000+1019):(n*20000+1519)),'k')
plot(TankPressure.time,TankPressure.data*0.145038-14.7,'-.k','linewidth',3)
xlabel('Time (s)'), ylabel('Pressure (psi)'), title('Tank Pressure')
legend('Experimental','Simulated')
set(gca,'FontSize',14,'fontWeight','bold')
set(gcf,'name',['Tank Pressure (' num2str(round(P_tank(1))) ' psi & L2 = '
num2str(round(L2,1)) 'mm) '])

```

Overlay Consecutive Experimental Results

```

load('C:\Users\gibsonj\Documents\MATLAB\Boost Converter\PBC Workspace Data -
Broken SMC CV (Paper)\02_Mar_2017_17_48_56.mat')
run('tube_system_params_Mar3_2017_smc.m');
sim('tube_system_adiabatic_expansion_Mar3_2017_smcCV')
%% Exhaust
figure, grid on, hold on
for n = 1:6
    time = t((n*20000+1019):(n*20000+1519)) - (n*20+1.018);
    plot(time,P_exh((n*20000+1019):(n*20000+1519))-14.7,'k')
    xlabel('Time (s)'), ylabel('Pressure (psig)'), title('Exhaust Pressure -
6 Trials')
    set(gca,'FontSize',14,'fontWeight','bold')
    yl = ylim(gca); yl(1)=-5; ylim(gca,yl);
end

```

```

%% Tank
figure, grid on, hold on
for n = 1:6
    time = t((n*20000+1019):(n*20000+1519)) - (n*20+1.018);
    plot(time,P_tank((n*20000+1019):(n*20000+1519)), 'k')
    xlabel('Time (s)'), ylabel('Pressure (psig)'), title('Tank Pressure - 6
Trials')
    set(gca, 'FontSize',14, 'fontWeight', 'bold')
end

```

Error Bar Plot Showing Range of Experimental Values and Simulated Results

```

sim = [2.0148, 3.0818, 3.104, 3.292, 3.7606, 3.7762, 3.8251, 3.581, 2.8628];
length = [142.24, 129.54, 116.84, 104.14, 91.44, 91.44, 78.74, 66.04, 53.34];

```

```

figure, grid on, hold on, xlim([50 150]), ylim([0 4.5])

```

```

exp_tests = [2.8958 2.6890 2.8269 2.7579 2.8269 2.4132
3.3784 2.7579 3.2405 2.8958 3.0337 3.2405
3.3784 3.3095 3.3784 3.3784 3.4474 3.3095
3.3784 3.3095 3.5853 3.5163 3.5163 3.2405
3.5163 3.7921 3.4474 3.4474 3.5163 3.3784
3.3784 3.3095 3.7921 3.6542 3.5163 3.4474
3.9300 3.8611 3.5853 3.8611 4.2748 3.5853
3.3784 3.8611 3.3784 3.6542 3.4474 3.4474
2.2063 1.8616 2.0684 1.7237 0 0];

```

```

for i = 1:8
    plot(length(i), mean(exp_tests(i,:)), 'ok', 'MarkerSize', 8)
    plot(length(i), sim(i), 'dk', 'MarkerSize', 8)
    errorbar(length(i), mean(exp_tests(i,:)), mean(exp_tests(i,:))-
min(exp_tests(i,:)), max(exp_tests(i,:))-mean(exp_tests(i,:)), 'LineWidth',1,
'Color', 'k');
end

```

```

plot(length(9), mean(exp_tests(9,1:4)), 'ok', 'MarkerSize',8)
plot(length(9), sim(9), 'dk', 'MarkerSize',8)
errorbar(length(9), mean(exp_tests(9,1:4)), mean(exp_tests(9,1:4))-
min(exp_tests(9,1:4)), max(exp_tests(9,1:4))-
mean(exp_tests(9,1:4)), 'LineWidth',1, 'Color', 'k')

```

```

legend('Experimental Average', 'Simulated Result', 'location', 'southeast')
title('Pressure Change During PBC Reclamation Event'), xlabel('L2 (mm)'),
ylabel('Pressure Change (kPa)')

```

```

ax1 = gca;
ax1.XTick = [50 60 70 80 90 100 110 120 130 140 150];
set(ax1, 'FontSize',14, 'fontWeight', 'bold')

```

```

ax2 = axes('Position', ax1.Position,
'XAxisLocation', 'top', 'YAxisLocation', 'right', 'Color', 'none', 'XTick', []);
set(ax2, 'YLim', [0 5.84], 'FontSize',14, 'fontWeight', 'bold')
ylabel('Energy Reclaimed (J)')

```

Extract Data from Target Machine, Plot, and Save

```
%% Extract data from target machine
clear;

% Attach to the target PC file system.
f = SimulinkRealTime.fileSystem;

% Open the file, read the data, close the file.
h = fopen(f, 'C:\gibson.dat');
data = fread(f, h);
f.fclose(h);

x = SimulinkRealTime.utils.getFileScopeData(data);

t = x.data(:, end);
P_tank = x.data(:, 1);
P_exh = x.data(:, 2);

%% Plot pressure results against time
figure
plot(t, P_tank, 'b', 'LineWidth', 2), grid on, hold on
plot(t, P_exh-14.7, 'r', 'LineWidth', 2)

set(gca, 'FontSize', 12)
xlim([t(1) t(end)]);
xlabel('Time (s)')
ylabel('Pressure (psi)')

%% Save workspace to file in format (day_month_year_hour_minute_second)
datetime=datestr(now);
datetime=strrep(datetime, ':', '_'); %Replace colon with underscore
datetime=strrep(datetime, '-', '_'); %Replace minus sign with underscore
datetime=strrep(datetime, ' ', '_'); %Replace space with underscore
save(datetime)
```

APPENDIX C: PROTOTYPE TECHNICAL DRAWINGS

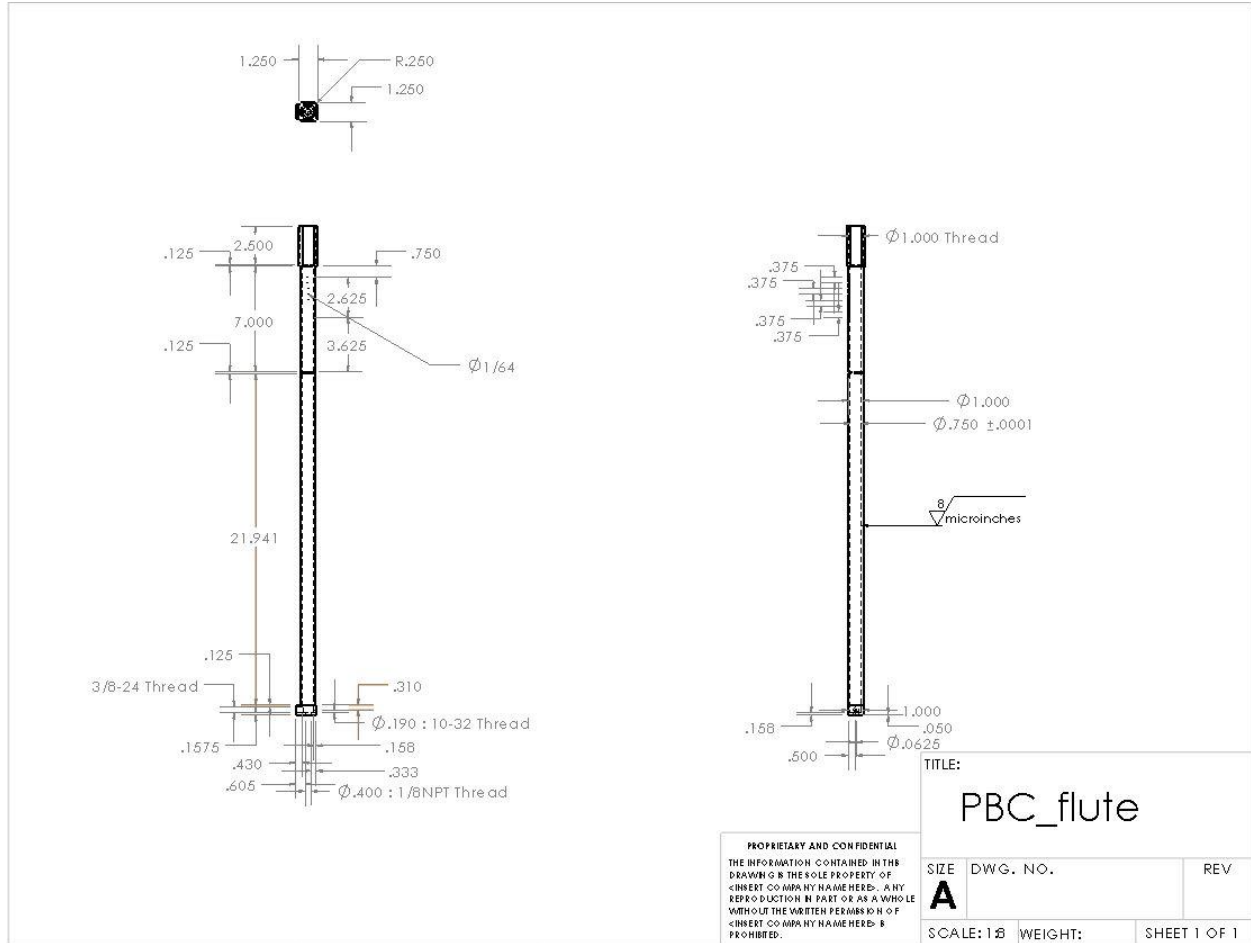


Figure C - 1: Pneumatic boost converter prototype technical drawing



Figure C - 2: Pneumatic boost converter 3D SolidWorks model

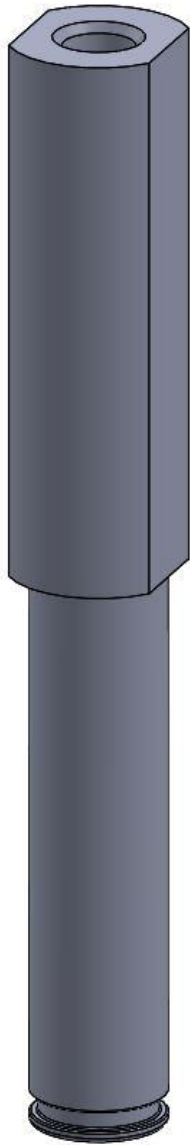


Figure C - 4: Adjuster 3D SolidWorks model

APPENDIX D: DATA ACQUISITION

Device Pinouts

Figure 8. NI PCI/PXI-6229 Pinout

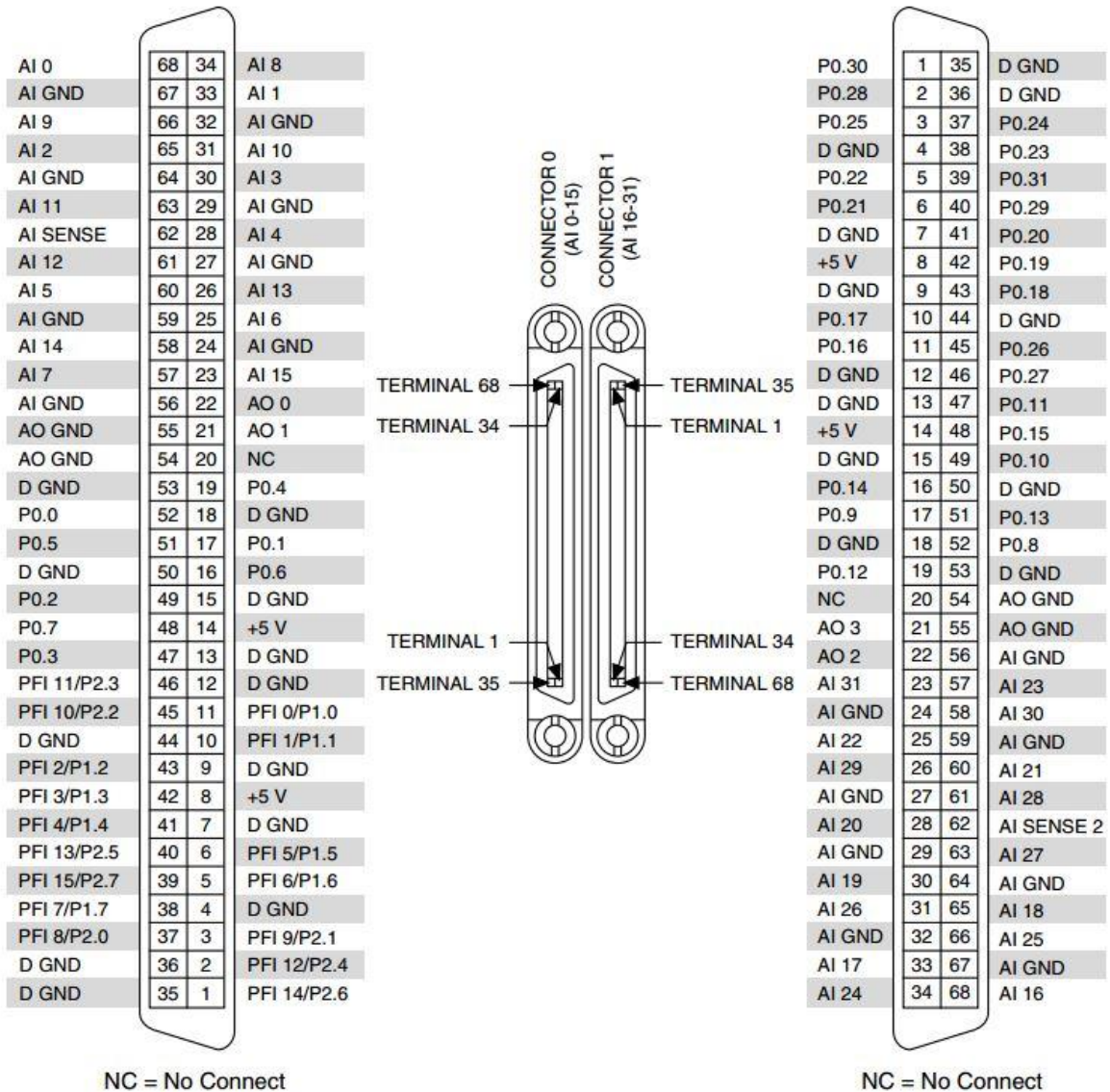


Figure D - 1: National Instruments data acquisition card pinout



5 VDC OUTPUT PRESSURE TRANSDUCER

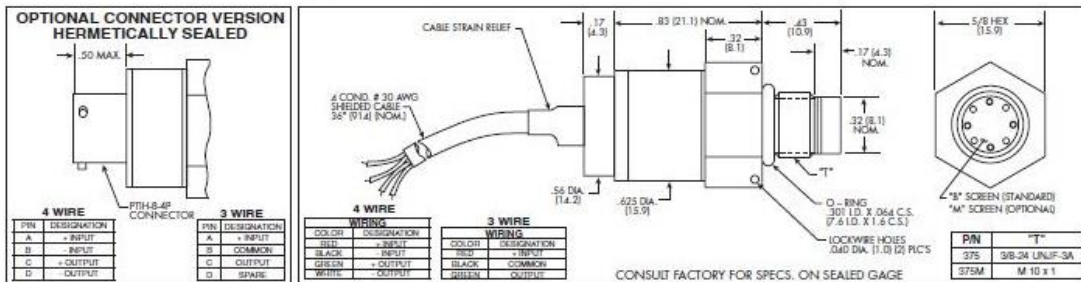
ETL-375 (M) SERIES

- 5 VDC Output
- Hybrid Microelectronic Regulator-Amplifier
- Patented Leadless Technology VIS®
- All Welded Construction
- Secondary Containment On Absolute And Sealed Gage Units
- Aerospace Quality Components
- 3/8-24 UNJF or M10 X 1 Thread
- 4 Wire (ETL-375) 3 Wire (ETL-300-375)



ETL-375 Series transducers are miniature, threaded instruments. The sensing sub-assembly is protected from mechanical damage by a solid screen which has been shown to have minimal influence on the frequency response of the sensor. The ETL Series uses Kulite's Patented Leadless Technology.

Incorporation of a Kulite proprietary electronics module within the main body of this product allows for operation from an unregulated power supply ranging from 12 ± 4VDC or 28 ± 4VDC with reverse polarity protection available upon request.



| | | | | | | | | | | |
|---------------|---|---|----------------------|----------------------|----------------------|-----------------------------------|----------------------|----------------------|----------------------|--|
| INPUT | Pressure Range | 1.7 25 | 3.5 50 | 7 100 | 17 250 | 35 500 | 70 1000 | 170 2500 | 350 BAR 5000 PSI | |
| | Operational Mode | Absolute, Gage, Sealed Gage | | | | | | | | |
| | Over Pressure | 2 Times Rated Pressure to 1000 PSI (70 BAR) 1.5 Times Rated Pressure Above 1000 PSI to a Max. of 6000 PSI (420 BAR) | | | | | | | | |
| | Burst Pressure | 3 Times Rated Pressure to a Max. of 10000 PSI (700 BAR) | | | | | | | | |
| | Pressure Media | All Nonconductive, Noncorrosive Liquids or Gases (Most Conductive Liquids and Gases - Please Consult Factory) | | | | | | | | |
| | Maximum Electrical Current | 25 mA | | | | | | | | |
| OUTPUT | Rated Electrical Excitation | 8 - 16 VDC | | | | 13 - 32 VDC | | | | |
| | Full Scale Reading | 5 VDC ± 150 mV | | | | 5 VDC ± 150 mV or 10 VDC ± 300 mV | | | | |
| | Output Impedance | 200 Ohms (Max.) | | | | | | | | |
| | Bandwidth (-3dB) | DC to 5 KHz | | | | | | | | |
| | Residual Unbalance | 0 to 100 mV (ETL-375) | | | | 200 mV ± 50 mV (ETL-300-375) | | | | |
| | Combined Non-Linearity, Hysteresis and Repeatability | ± 0.1% FSO BFSL (Typ.), ± 0.5% FSO (Max.) | | | | | | | | |
| | Resolution | Infinitesimal | | | | | | | | |
| | Natural Frequency of Sensor Without Screen (KHz) (Typ.) | Greater Than 400 KHz | | | | | | | | |
| | Acceleration Sensitivity % FS/g Perpendicular | 1.9x10 ⁻³ | 1.0x10 ⁻³ | 5.2x10 ⁻⁴ | 2.2x10 ⁻⁴ | 1.1x10 ⁻⁴ | 6.2x10 ⁻⁵ | 2.6x10 ⁻⁵ | 1.5x10 ⁻⁵ | |
| | Insulation Resistance | 100 Megohm Min. @ 50 VDC | | | | | | | | |
| ENVIRONMENTAL | Operating Temperature Range | -65°F to +250°F (-55°C to +120°C) | | | | | | | | |
| | Compensated Temperature Range | 0°F to +212°F (-18°C to +100°C) Other Ranges Quoted on Request | | | | | | | | |
| | Thermal Zero Shift | ± 1% FS/100° F (Typ.) | | | | | | | | |
| | Thermal Sensitivity Shift | ± 1% /100° F (Typ.) | | | | | | | | |
| | Linear Vibration | 100g Peak, Sine up to 5000 Hz | | | | | | | | |
| PHYSICAL | Humidity | 100% Relative Humidity | | | | | | | | |
| | Mechanical Shock | 100g half Sine Wave 11 msec. Duration | | | | | | | | |
| | Electrical Connection | 4 Conductor 30 AWG Shielded Cable 36" Long | | | | | | | | |
| | Weight | 24.5 Grams (Max.) Excluding Cable | | | | | | | | |
| PHYSICAL | Pressure Sensing Principle | Fully Active Four Arm Wheatstone Bridge Dielectrically Isolated Silicon on Silicon Patented Leadless Technology | | | | | | | | |
| | Mounting Torque | 80 Inch-Pounds (Max.) | | | | | | | | |

Note: Custom pressure ranges, accuracies and mechanical configurations available. Dimensions are in inches. Dimensions in parenthesis are in millimeters. All dimensions nominal. (M) Continuous development and refinement of our products may result in specification changes without notice. Copyright © 2014 Kulite Semiconductor Products, Inc. All Rights Reserved. Kulite miniature pressure transducers are intended for use in test and research and development programs and are not necessarily designed to be used in production applications. For products designed to be used in production programs, please consult the factory.

KULITE SEMICONDUCTOR PRODUCTS, INC. • One Willow Tree Road • Leonia, New Jersey 07605 • Tel: 201 461-0900 • Fax: 201 461-0990 • <http://www.kulite.com>

Figure D - 2: Kulite ETL-375 pressure sensor data sheet

Pressure transmitters SPTW

Technical data

FESTO

| Output, additional data | |
|----------------------------------|-----|
| Protection against short circuit | Yes |

| Electronic components | | | |
|-----------------------------|-----|-----------------------|-----------|
| SPTW-...- | | A | VD |
| Operating voltage range DC | [V] | 8 ... 30 | 14 ... 30 |
| Reverse polarity protection | | For operating voltage | |

| Electromechanical components | |
|------------------------------|--|
| Electrical connection | Plug M12x1, 4-pin To EN 60947-5-2 Round design |
| Plug housing material | PA |

| Mechanical components | |
|--|--|
| Type of mounting | Via female thread Via accessories |
| Mounting position | Any |
| Pneumatic connection | G1/4 |
| Product weight | [g] 80 |
| Housing materials | High-alloy stainless steel PA VMQ (silicone) |
| Materials in contact with the medium ¹⁾ | High-alloy stainless steel |

| Immissions/emissions | |
|--|------|
| Protection class | IP67 |
| Corrosion resistance class CRC ²⁾ | 4 |

1) Group CrNiMo: 316L, from measurement range 10 bar the membrane is composed of 13-8-PH

2) Corrosion resistance class 4 according to Festo standard 940 070
Components subject to particularly high corrosion stress. Parts used with aggressive media, e.g. in the food or chemical industry. These applications should be supported with special tests with the media if required.



| Pin allocation | | | SPTW-...-VD | | |
|---|-----|-----------------------------------|---|-----|-------------------------|
| SPTW-...-A | | | SPTW-...-VD | | |
| Plug M12x1, 4-pin | Pin | Meaning | Plug M12x1, 4-pin | Pin | Meaning |
|  | 1 | Operating voltage U_0 /signal + |  | 1 | Operating voltage U_0 |
| | 3 | 0 V/signal - | | 3 | 0 V |
| | | | | 4 | Analogue output |

Figure D - 3: Festo SPTW pressure sensor data sheet